frontiers | Frontiers in Earth Science

ORIGINAL RESEARCH
published: 08 April 2022
doi: 10.3389/feart.2022.867616

Sedimentary Environment and Enrichment of Organic Matter During the Deposition of Qiongzhusi Formation in the Upslope Areas—A Case Study of W207 Well in the Weiyuan Area, Sichuan Basin, China

Lei Zhao[1,2], Shugen Liu[1,3], Guoqin Li[2], Menglin Zhang[2], Xiao Liang[2], Junxiang Li[4] and Jianliang Xu[2]*

[1]State Key Laboratory of Oil and Gas Reservoir Geology and Exploitation, Chengdu University of Technology, Chengdu, China, [2]CCDC Geological Exploration and Development Research Institute, CNPC, Chengdu, China, [3]Xihua University, Chengdu, China, [4]Shale Gas Project Department of Chuanqing Drilling Engineering, CNPC, Chengdu, China

OPEN ACCESS

Edited by:
Kun Zhang,
Southwest Petroleum University, China

Reviewed by:
Xiong Ding,
Southwest Petroleum University, China
Shuo Cao,
China University of Geosciences, China
Qingbo Wang,
Sinopec, China

***Correspondence:**
Xiao Liang
liangx_dyy@cnpc.com.cn

Specialty section:
This article was submitted to Geochemistry, a section of the journal Frontiers in Earth Science

Received: *01 February 2022*
Accepted: *21 February 2022*
Published: *08 April 2022*

Citation:
Zhao L, Liu S, Li G, Zhang M, Liang X, Li J and Xu J (2022) Sedimentary Environment and Enrichment of Organic Matter During the Deposition of Qiongzhusi Formation in the Upslope Areas—A Case Study of W207 Well in the Weiyuan Area, Sichuan Basin, China. Front. Earth Sci. 10:867616. doi: 10.3389/feart.2022.867616

For a more in-depth analysis on the marine chemical condition during the earliest Cambrian, mechanism of organic matter enrichment and exploration potential of shale gas resources, based on the petrology, organic geochemistry, and elemental characteristics of the W207 Well, this study discuss the Early Cambrian paleo-ocean environment and factors controlling of organic matter enrichment during the deposition of black strata Qiongzhusi Formation in the upslope areas, southwestern Sichuan Basin, Yangtze Block, China. The sedimentary cycles show that during the depositon of fine-grained Qiongzhusi Fm, interactive cycles of multiple deep-water and shallow-water shelf developed, and were controlled by the rise and fall in sea level. In particular, the slope turbidite (fan) and gravity flow sediments indicate that the shallow-water shelf facies were dominant in the upslope area (SW Sichuan Basin), where not in deep water for a long time, and the sedimentary thickness of the organic rich black shale was limited. Evidence from organic geochemistry indicates that the organic matter of the Qiongzhusi Fm from the W207 Well was mainly of type I kerogen, with a high degree of thermal evolution, little residual hydrocarbon, and low capacity for hydrocarbon generation. The redox parameters indicate that the marine environment on the upslope was medium restrictive, with some upwelling. The seawater had undergone a transformation according to anoxic–oxidic. Therefore, paleo-ocean productivity in the upslope area was generally low, and exhibited a prominent downward trend from bottom to top. Given its high risk of exploration, the authors suggest that the direction of shale gas resource evaluation should change to the intracratonic sag (downslope) area, which is characterized by deep-water shelf facies.

Keywords: Early Cambrian, upslope area, Qiongzhusi Fomation, paleo-ocean environment, mechanism of organic matter enrichment

INTRODUCTION

In the Early Cambrian (541–514 Ma), a thick layer of shale that was rich in marine organic matter was deposited on the Upper Yangtze Platform (Sichuan Basin and its periphery) to form the Maidiping Fm–Qiongzhusi Fm. This area has since been an important potential site for the exploration of shale gas, and forms a major series after the Wufeng Fm–Longmaxi Fm (Hu et al., 2012; Huang et al., 2012; Sun et al., 2012; Zhang et al., 2020; Liang et al., 2021). The Early Cambrian is also a key period for the transformation of the marine environment and biological life in geological history. With the gradual increase in atmospheric marine oxygen in this period, multicellular organisms began to appear and flourish, forming the Cambrian Bio-radiation Event (Xiao et al., 1998; Zhu et al., 2008; Raven et al., 2021). Changes in the marine environment play a decisive role in the evolution of life (Bush et al., 2007; Shu et al., 2014), and are closely related to the formation of organic matter-rich shale (Zhao et al., 2020; Zhou et al., 2020). The enrichment of organic matter in high-quality marine source rocks is controlled by such factors as the terrigenous input, hydrodynamic conditions, redox conditions, and productivity in a sedimentary environment (Jin et al., 2020). Understanding the sedimentary environment of the Qiongzhusi Fm and exploring its mechanism of enrichment of organic matter are thus important for assessing its value as a resource for shale gas.

The characteristics of terrigenous input are closely related to the paleoclimate and paleoweathering conditions of the source area (Taylor and Mclennan., 1985). The degree of chemical weathering of surface rocks is mainly affected by temperature and humidity (Parker., 1970). Hot and humid climates promote the chemical weathering of rocks, while cold and dry climates are not conducive to it (Nesbitt and Young., 1982). In recent years, the chemical index of alteration (CIA), weathering index of Parker (WIP), chemical index of weathering (CIW), plagioclase index of alteration (PIA), Mg index (MgI), and mafic index of alteration (MIA) (Parker, 1970; Nesbitt and Young, 1982; Nesbitt et al., 1996; Fedo et al., 1995; Babechuk et al., 2014; Craig et al., 2017) have been widely used to reflect the degree of weathering and the paleoclimate.

In the hydrodynamic environment discrimination conditions, based on the unique geochemical characteristics of Mo and U elements and the influence of Mn, Fe and other particles on the enrichment of Mo elements, and using the corresponding relationship between Mo/TOC value in sediments and Mo element concentration in seawater, Mo-TOC charts (Algeo et al., 2008), U_{EF}-Mo_{EF} covariant model (Algeo and Tribovillard, 2009) and Co*Mn plate (Sweere et al., 2016)for distinguishing the retention degree of sediments in different marine environments and open/upwelling environment are established. Because the Co*Mn model is not as precise as the Mo-TOC and U_{EF}-Mo_{EF} models in the identification of the degree of retention, and cannot distinguish among the redox conditions of seawater, it can be used as a supplement for the development of the Mo-TOC and U_{EF}-Mo_{EF} covariant models. The extensive use of the three methods can be used to distinguish among three marine environments, those with non-retention, weak retention, and strong retention, such as the Black Sea that has strong retention (Brumsack, 1989; Baturin, 2011) and the Cariaco Basin with weak retention (Piper and Dean, 2002).

The enrichment of organic matter in sediments is also closely related to the redox conditions of the sedimentary environment and the size of primary productivity in the ocean (Algeo et al., 2008; Zhang et al., 2016). Traditionally, oxygen content in the earlier Cambrian ocean is considered to have been close to that in the modern ocean (Logan et al., 1995; Scott et al., 2008), but the latest research shows that the redox environment in the Early Cambrian was in a highly stratified state, with oxidized water on the surface and anoxic iron deeper below. Dynamically changing sulfide seawater persisted between them (Chang et al., 2016; Zhu et al., 2018; Jin et al., 2020). The paleo-ocean redox conditions controlled the degree of enrichment of trace elements in the sedimentary rocks (Guo et al., 2007; Och et al., 2013). By analyzing the ratios of trace elements (U, V, Mo, V/Cr, and U/Th) and factors influencing their enrichment (through U_{EF}, V_{EF}, MO_{EF}, etc.), the paleo-marine environment can be reconstructed (Guo et al., 2007; Och et al., 2013; Pi et al., 2013; Spangenberg et al., 2014; Zhao et al., 2020). The content of some biologically essential nutrient elements (such as Cu, Zn, P, and Ni) in sedimentary rocks can help evaluate paleo-productivity (Shen et al., 2015; Reinhard et al., 2016).

Deployed by the CNPC and cored for the entire section, the W207 Well is a special evaluation well of the Qiongzhusi Fm in the southwestern Sichuan Basin of China. It provides an important basis for studying the sedimentary environment and the mechanism of enrichment of organic matter in the Qiongzhusi Fm at shallow-water shelf facies (upslope area). This study analyzes the total organic carbon (TOC) content, organic carbon isotopic composition ($\delta^{13}C_{org}$), and major and trace element contents of the Qiongzhusi Fm from the W207 Well in the Weiyuan area. We used the factors influencing the redox environment (U/Th, V/Cr, C_{org}/P, U_{EF}, V_{EF}, Mo_{EF}, etc.) and indicators of paleo-ocean productivity (Cu, Zn, Ni, Ba_{bio}, etc.) to reconstruct the paleo-ocean environment in the upslope area on the west side of the Mianyang-Changning Intracratonic Sag. Further, we analyzed the factors controlling the enrichment of organic matter of the Qiongzhusi Fm, and clarify its potential as a source of marine shale gas in the southern Sichuan Basin.

GEOLOGICAL SETTING

Tectonic Characteristics

The W207 Well (Weiyuan area) is located in the west side of the middle segment of the Mianyang–Changning Intracratonic Sag. The area belongs to the Leshan–Weiyuan slope and transitions into the interior of the intracratonic sag to the East. Owing to the long-term and transgressive sequential marine clastic-carbonate deposition of the Doushantuo Fm (*Zds*) and the carbonate platform deposition of Dengying Fm (Z_2dn) in the Late Sinian, the Upper Yangtze Platform (Sichuan Craton) had an extension in the earlier Cambrian. Taking the formation of the Mianyang–Changning Intracratonic Sag as the main signal of Xingkai Taphrogenesis (Liu et al., 2013), prominent paleogeographic differentiation began to appear in the Upper Yangtze Platform in the earlier Cambrian (Hou et al., 2017).

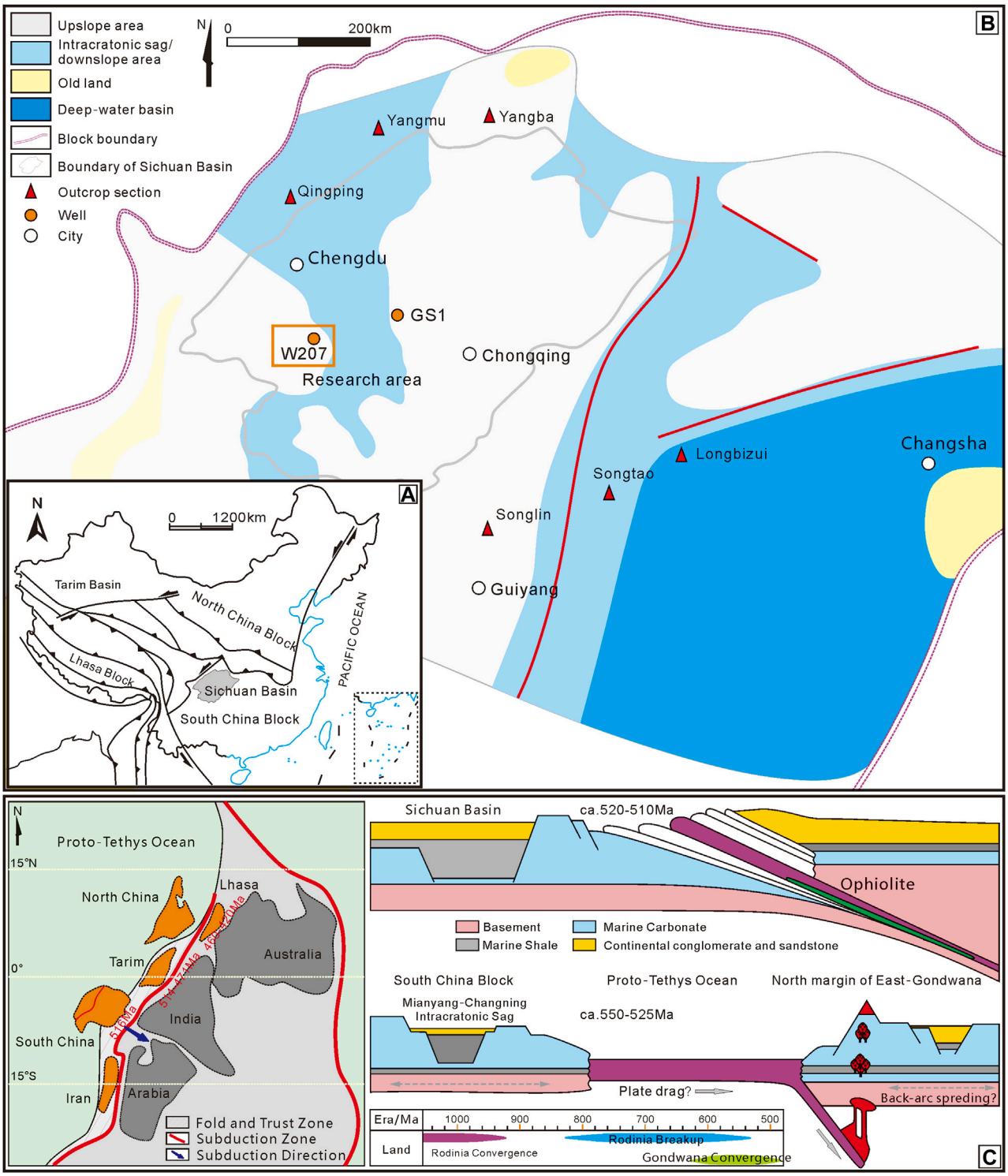

FIGURE 1 | (A) Simplified map of China that shows the location of the Sichuan Basin (gray), South China Block. **(B)** Early-Cambrian tectonic paleogeography of the Upper Yangtze Region (modified from Li et al., 2019 and Ding et al., 2021). The W207 Well is located at west side of Mianyang-Changning Intracratonic Sag. **(C)** Aggregation kinetic model between Yangtze and Gondwana (Arabia) in the Early Paleozoic.

Representing the initial stage of extension (542–529 Ma), the Lower Cambrian Maidiping Fm is only locally developed in the central and western, western margin, and southwestern margins of the Sichuan Basin. In the Upper Yangtze Platform and most areas around it, the Qiongzhusi Fm (multiple sets of synonymous strata, also known as Jiulaodong Fm, Qingping Fm, Guojiaba Fm, Shuijingtuo Fm, and Niutitang Fm) was deposited at the peak stage of extension (521–514 Ma), which appeared as unconformable contact with the underlying Dengying Fm. Therefore, during the sedimentary period of Qiongzhusi Fm, the Upper Yangtze Platform can be divided into three special structural areas from west to east: upslope area, intracratonic sag or downslope area, and a deep basin area (**Figure 1B**).

Despite controversial subduction-collage mode, with complete disintegration of Rodinia gradually converged to Gondwana in the Late Neoproterozoic-Early Paleozoic, previous evidence suggests that the South China Block gradually subducted from the northwest edge of Rodinia to the East Gondwana (Jiang et al., 2003; Li et al., 2008, 2013). The prominent non-conformity between the Cambrian and the Ordovician on the western margin of the Yangtze Block and the latest detrital zircon U-Pb age/Lu-Hf isotope reveal that a large number of Pan-African young zircons (ca. 0.55–0.52 GA) are related to the provenance of the East African Orogenic Belt in the Cambrian on the western margin of the Yangtze Block (Yao et al., 2015; Chen et al., 2018). The western margin of the Yangtze is thus more likely to be collaged with the northern margin of East Gondwana (low equatorial latitude) (**Figure 1C**). Taking the Sichuan Basin as an important benchmark, the Yangtze Craton, which dissociated in the Proto-Tethys Ocean, had inherited the weak structural pattern of the basement and continued to be tensioned by the periphery of the craton. As a result, a tectono-depositional differentiation was formed in the craton during the Sinian (Ediacaran)–Cambrian transition period. Considering the boundary characteristics of the Sinian (Ediacaran)–Cambrian as the benchmark in a similar way, the South China (Yangtze) platform before the deposition of Qiongzhusi Fm was in three special sedimentary facies from the northwest to the southeast, including the platform facies, slope transition facies, and deep-water basin facies (Li et al., 2020; Ding et al., 2021). Considering plate tectonics, the uplift groove pattern of the Sichuan Basin and its periphery during the Sinian Cambrian transition period was mainly formed in the stage of convergence of the Gondwana continent. During the subduction of the Proto-Tethys Ocean, oceanic crust and plates were dragged by the driving force of plate subsidence, and episodic uplift and rifting events might have occurred on the shallow surface of the crust (Wang et al., 2016; Li et al., 2019; Wang, 2020). After South China and Gondwana completely collaged in 516 Ma, the compression background caused the intracratonic sag fill quickly with sediments.

Depositional and Stratum-Related Characteristics

The Qiongzhusi Fm is a set of shelf facies of shale deposit with a thickness of 259.9 m. The pulveryte interval of the W207 Qiongzhusi Fm can be divided into three continuously superimposed third-order sequences. Controlled by the rise and fall in sea level, the characteristics of the sedimentary cycles show that interactive cycles of conversion between multiple deep-water shelf and shallow-water shelf developed (**Figure 2**). The lithology of the strata of the deep-water shelf facies was mainly black carbonaceous mudstone/shale, black silty mudstone/shale, and black mud/shale mixed with a small amount of stone coal, rich in organic matter. It developed a horizontal bedding, and represented deep seawater and a weak hydrodynamic force.

The shallow-water and semi-deep-water shelves were also below the stormed wave base. The seawater was relatively quiet, with hydrostatic low-energy deposition in this environment. The lithology of the sediment is mainly black argillaceous siltstone, black silty mudstone, and grayish-green lithic feldspar sandstone, with fine-grained sandstone mixed with it. The overall grain size was fine, the horizontal bedding was developed, and a small amount of cross-bedding could be seen locally. In this environment, calcareous siltstone, thin-layer micrite limestone, and silty limestone were also deposited.

The sedimentary thickness of the deep-water shelf facies and shallow-water shelf facies was quite different in the W207 Well. The deep-water shelf facies ranged from several meters to tens of meters, and generally decreased in thickness from bottom to top. The total thickness is 67m, accounting for 25.8%. Although there was no evidence of benthos in the strata under this sedimentary environment, it can be judged to be deep-water, low-energy, and anoxic deposition due to a small amount of bacteria and algae, siliceous sponge bone needles, and radiolaria. Moreover, the bottom of Qiongzhusi Fm in the W207 Well is characterized by typical slope of turbidite fan deposition, mainly silty deposition, interbedded with carbonaceous shale deposited in the continental shelf. The rhythmic occurrence of D and E segments of the typical Bouma sequence, and development of small sand bedding and horizontal bedding can be seen locally, which is a consequence of deposition due to gravitational flow (**Figure 3**). We infer that the Qiongzhusi Fm in the upslope area is dominated by shallow-water shelf deposits, and slope turbidites have developed. The Weiyuan area where W207 is located has not been in the deep water area close to the intracratonic sag for a long time. The sedimentary thickness of the organic-rich black shale is thus limited. Deep-water shelf facies have mainly developed on the east of the Weiyuan area, close to the Mianyang–Changning Intracratonic Sag. We think that organic-rich shale is thin in the west and gradually thickens eastward.

EXPERIMENTS METHODS AND DATA SOURCES

A total of 44 samples, including siliceous shale, black shale, dark-gray argillaceous siltstone, and gray siltstone, were collected from the earliest Cambrian black strata of the Qiongzhusi Fm from the W207 Well in the southwestern Sichuan Basin (**Figure 2**).

FIGURE 2 | Macroscopic characteristics of cores in the whole section of Qiongzhusi Fm, W-207 Well. The Qiongzhusi Fm can be divided into three third-order sequences. SQI: First member of Qiongzhusi Fm ($\epsilon_1 q^1$), 3,242.13–3,135.94 m; SQ II: Second member of the Qiongzhusi Fm ($\epsilon_1 q^2$), 3,135.94–3,043.65 m; SQ III: Third member of the Qiongzhusi Fm ($\epsilon_1 q^3$), 3,043.65–3,000.59 m.

Total Organic Carbon Content and Pyrolysis

Measurements of total organic carbon content (TOC) were performed using a LECO CS-344 carbon/sulfur analyzer with an analytical accuracy of ±0.5%. About 80–120 mg powder (120 mesh) of each sample was weighed and treated with 10% HCl to thoroughly remove the carbonates. Subsequently, the residue was filtered and rinsed with H_2O to remove chlorides before introducing the dried residue to the C/S analyzer. Pyrolysis was performed by using a Rock-Eval VI analyzer.

The pyrolysis process lasted 12 min. The initial temperature was 90°C, and the constant temperature was maintained for 2 min to obtain the S_0 peak. In the first stage, the temperature was 300°C, and constant temperature was maintained for 3 min to obtain the S_1 peak. In the second stage, within 6 min, the heating rate was 50°C/min, and constant temperature was maintained at 600°C for 1 min to get the S_2 peak. The T_{max} was corresponding peak temperature of S_2 during rock pyrolysis, indicating the thermal maturity of organic matter.

Bulk Organic Carbon Isotopic Ratios ($\delta^{13}C_{org}$)

The measurements of $\delta^{13}C_{org}$ were carried out on carbonate-free samples using an elemental analyzer (EA) coupled with a flow interface that automatically transferred carbon dioxide gas into a Finnigan delta-plus mass spectrometer. The samples included bulk oil, pure bitumen, and kerogen from the source rocks. Casein was used as the external standard (Elemental Microanalysis Ltd.) with a value of $\delta^{13}C_{V\text{-}PDB}$ of −26.98‰. The results were reported in terms of per mil relative to VPDB (i.e., Vienna Peedee Belemnite), and the reproducibility of the replicate analyses was ±0.3‰.

Main Element Analysis

The 44 samples from Qiongzhusi Fm in Well W207 were pretreated by the glass melt method and then analyzed by a Primus II X-ray fluorescence spectrometer (XRF). The processing flow of major element analysis was as follows: 1) The 200 mesh samples were placed in a 105°C oven to dry for 12 h; 2) One Gram of the dried powder sample was weighed and placed in a ceramic crucible, and then heated to 1,000°C for calcination for 2 h; 3) Weigh 0.6 g sample, 0.3 g NH_4NO_3 oxidizer and 0.6 g accelerant ($Li_2B_4O_7$/$LiBO_2$/LiF = 9/2/1), then place them in a platinum crucible and mix them evenly, melt them at 1,050°C, cool them after complete melting, take out the glass sheet and test them on the machine. The analysis accuracy is better than 2%.

Trace Element Analysis

The concentrations of trace elements in the bitumen and potential source rocks were determined using inductively coupled plasma mass spectrometry (ICP-MS; Agilent 7,700×) combined with inductively coupled plasma atomic emission spectrometry (ICP-AES; Agilent VISIA). The sample powders (200 mesh) were first prepared by dissolution using a mixture of four acids (HNO_3 + $HClO_4$ + HF + HCl). The organic-rich samples were combusted in a muffle oven at 750 C to remove

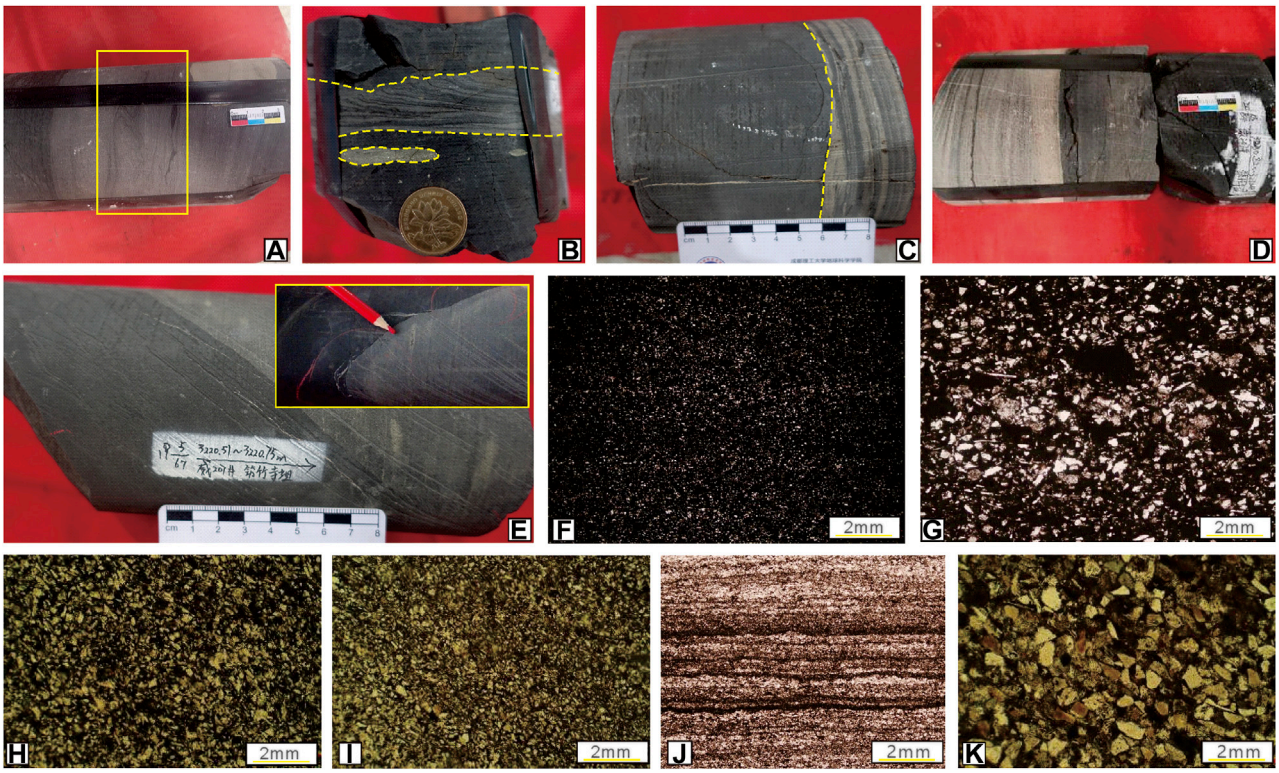

FIGURE 3 | Petrological characteristics of Qiongzhusi Fm, W-207 Well. **(A)** W207 Well, 3,232.80m, at the bottom of Qiongzhusi Fm, soft sediment deformation **(B)** W207 Well, 3,231.66 m, at the bottom of Qiongzhusi Fm, cross bedding and lenticular pyrite nodules **(C)** W207 Well, 3,186.30 m, the lower part of Qiongzhusi Fm, black shale alternates with gray laminar calcareous shale **(D)** W207 Well, at the bottom of Qiongzhusi Fm, black shale is in contact with gray black siltstone, suspected of Bouma sequence **(E)** W207 Well, 3,220.57m, the lower part of Qiongzhusi Fm, black shale is in contact with gray elliptic calcareous nodules **(F)** W207 Well, 3,242.29 m, silty calcareous mudstone **(G)** W207 Well, 3,242.29 m, silty calcareous mudstone, with a large amount of carbonate clasts **(H)** W207 Well, 3,149.58 m, the middle part of Qiongzhusi Fm, mainly composed of silty mudstone and with little argillaceous siltstone **(I)** W207 Well, 3,088.35 m, the upper part of Qiongzhusi Fm, felsic siltstone **(J)** W207 Well, 3,055.91 m, the upper part of Qiongzhusi Fm, normal grain sequence, suspected parallel bedding development, dolomitic lithic siltstone laminated siliceous shale and carbonaceous shale with the characteristics of turbidite deposition **(K)** W207 Well, 3,000.59 m, silty argillaceous very fine-grained quartz sandstone.

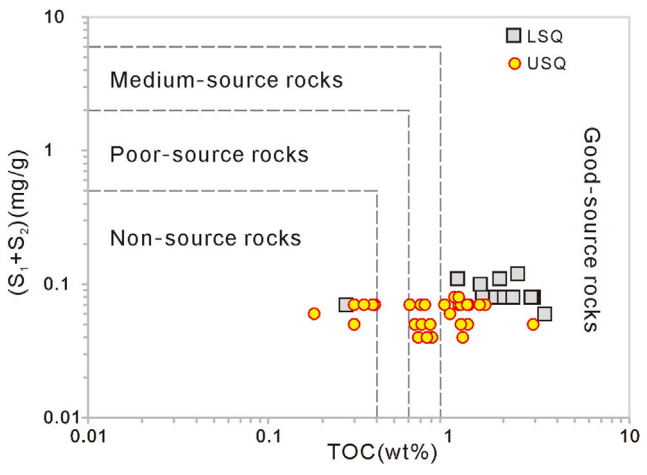

FIGURE 4 | Characteristic map of total organic carbon (TOC) vs. S_1+S_2 from the Qiongzhusi Fm, W-207 Well. LSQ: lower section of Qiongzhusi Fm (3,242.42–3,177.64 m); USQ: upper section of Qiongzhusi Fm (3,161.69–3,000.59 m).

organic matter before dissolution by acids. The analytical procedure detailed by Pi et al. (2013) was followed. The standard deviation of the elemental concentrations was <10%. Bulk trace elements were analyzed at the ALS Laboratory Group's Mineral Division, ALS Chemex, in Guangzhou, China (**Table 2**).

The enrichment factors (EF) of redox-sensitive elements were calculated by $X_{EF} = [(X/Al)_{sample}/(X/Al)_{PAAS}]$, where X and Al represent the contents of the specified elements and aluminum elements, respectively. The reference standard was the content of elements in post-Archean Australian average shale (PAAS). The biogenic Ba was calculated as $Ba_{bio} = Ba_{sample} - (BA/Al)_{PAAS} \times Al_{sample}$, and the reference standard here was also the content of elements in PAAS (Taylor and Mclennan, 1985).

RESULTS AND DISCUSSION

Hydrocarbon Potential

Total Organic Carbon Content

The organic carbon content (TOC) is the basic parameter in assessing source rocks for shale gas. On the one hand, only when

TABLE 1 | Organic geochemical parameters of Qiongzhusi Fm, W-207 Well.

Samples	Depth (m)	TOC (wt%)	$\delta^{13}C_{org}$ (‰)	S_1 (mg/g)	S_2 (mg/g)	S_3 (mg/g)	T_{max} (°C)	HI	OI
W207-44	3,000.59	0.39	−30.94	0.02	0.05	0.04	329	10	8
W207-43	3,010.55	0.65	−30.72	0.01	0.04	0.05	608	6	7
W207-42	3,015.03	0.70	−30.65	0.02	0.05	0.06	317	6	7
W207-41	3,026.19	0.68	−30.44	0.01	0.03	0.07	610	4	10
W207-40	3,035.38	0.81	−30.55	0.01	0.03	0.07	611	3	7
W207-39	3,043.95	1.28	−30.57	0.01	0.04	0.09	611	3	6
W207-38	3,055.91	0.30	−30.82	0.02	0.05	0.07	342	14	19
W207-37	3,062.45	0.30	−30.8	0.02	0.03	0.05	609	8	12
W207-36	3,080.51	0.38	−31.15	0.02	0.05	0.09	441	11	19
W207-35	3,088.35	0.61	−31.66	0.02	0.05	0.08	320	6	10
W207-34	3,103.15	0.76	−31.84	0.01	0.03	0.1	332	3	9
W207-33	3,110.67	1.08	−31.87	0.02	0.06	0.03	350	4	2
W207-32	3,115.74	1.30	−31.83	0.02	0.05	0.08	327	3	6
W207-31	3,130.65	2.94	−31.56	0.02	0.03	0.1	611	1	3
W207-30	3,138.43	1.20	−31.57	0.01	0.03	0.08	612	2	5
W207-29	3,142.57	1.14	−32.07	0.02	0.05	0.14	375	4	10
W207-28	3,147.64	1.60	−32.01	0.02	0.05	0.08	612	3	5
W207-27	3,149.58	1.17	−32.05	0.02	0.05	0.09	352	3	6
W207-26	3,151.99	1.02	−31.91	0.02	0.04	0.12	334	3	10
W207-25	3,157.82	0.71	−31.83	0.01	0.04	0.14	611	4	15
W207-24	3,159.56	1.27	−31.96	0.02	0.05	0.1	332	3	7
W207-23	3,161.69	1.49	−32.35	0.02	0.05	0.07	316	3	4
W207-22	3,177.64	0.18	−31.42	0.01	0.05	0.2	375	21	83
W207-21	3,179.10	0.79	−33.27	0.01	0.04	0.05	612	4	5
W207-20	3,181.40	0.95	−33.48	0.02	0.05	0.05	332	4	4
W207-19	3,184.63	1.17	−33.77	0.01	0.04	0.05	612	3	3
W207-18	3,186.42	0.34	−32.8	0.02	0.05	0.2	351	11	45
W207-17	3,187.41	1.14	−33.89	0.02	0.06	0.03	612	4	2
W207-16	3,189.12	0.74	−33.79	0.02	0.05	0.03	612	5	3
W207-15	3,221.05	1.94	−32.79	0.02	0.06	0.05	611	3	2
W207-14	3,222.01	2.94	−32.91	0.02	0.06	0.09	372	2	3
W207-13	3,224.51	2.41	−32.6	0.05	0.07	0.24	365	1	5
W207-12	3,226.01	2.87	−32.86	0.02	0.06	0.06	612	2	2
W207-11	3,226.94	2.27	−33.03	0.02	0.06	0.06	612	2	2
W207-10	3,228.38	1.72	−33.42	0.02	0.06	0.07	612	3	3
W207-09	3,230.18	1.12	−33.56	0.02	0.09	0.06	437	6	4
W207-08	3,230.82	0.27	−32.94	0.01	0.06	0.19	612	17	53
W207-07	3,233.63	1.54	−34.29	0.02	0.06	0.05	365	3	3
W207-06	3,235.14	1.50	−34.38	0.02	0.08	0.06	375	4	3
W207-05	3,237.58	1.92	−34.43	0.02	0.09	0.07	612	4	3
W207-04	3,238.27	1.57	−34.47	0	0	0.06	479	0	3
W207-03	3,240.11	1.78	−34.59	0	0	0.15	293	0	7
W207-02	3,241.19	3.31	−34.95	0	0	0.07	479	0	2
W207-01	3,242.29	3.41	−34.81	0.02	0.04	0.1	361	1	2

the abundance of organic matter reaches a certain degree can it have sufficient capacity for hydrocarbon generation. On the other hand, once the organic matter has been converted into hydrocarbons, certain storage space is formed to store hydrocarbons, and the residual organic carbon reaches a certain amount such that it has the ability to adsorb hydrocarbon gases, which become shale gas reservoirs when the two parts of gas reach a certain amount. They then become shale gas reservoirs. Researchers have different views of this based on regions and strata. The standard of organic carbon content in the Qiongzhusi Fm, with high maturity in south China, can be reduced to 0.5–1.0% (Zhang et al., 2002).

The TOC of 44 samples from W207 in Qiongzhusi Fm ranged from 0.18% to 3.41%, with an average of 1.31% (**Table 1**). The section with high TOC (TOC > 1%) was 130 m (**Table 1**). The TOC content of the LSQ black rocks (3,242.42–3,177.64 m) ranged from 0.18% to 3.41% (average of 1.63%) while that of USQ black rocks (3,161.69–3,000.59 m) ranged from 0.30% to 2.94% (average of 0.99%). This considerable difference may relate to the special sedimentary backgrounds of the lower and upper strata, which control the enrichment and preservation of organic matter by adjusting nutrient input and water chemistry. The data on W207 show that the common abundance of residual organic matter in this well. There were only two sets of sections with relatively high TOC, corresponding to the bottom of $\epsilon_1 q^1$ and middle of $\epsilon_1 q^{2\text{-}3}$, respectively. This is consistent with the two sets of high-GR sections.

The sum of S_1 and S_2 yields is widely used to indicate the hydrocarbon potential, and decreases sharply with increasing

quantity of petroleum generated and expelled from the source rocks (Peters and Cassa, 1994). Conversely, TOC content is the main source of hydrocarbon generation, and undergoes little change in weight percent when oil and gas are generated (Lu et al., 2012; He et al., 2020b). By considering the low S_1 and S_2 yields (mainly ranging from 0.04 mg/g to 0.12 mg/g) due to the generation and expulsion of a large amount of hydrocarbons under a high degree of thermal evolution, the TOC content was applied to assess the degree of enrichment of organic matter within the source rocks (Peters and Cassa, 1994; Peters et al., 2005; Lu et al., 2012).

However, these ranges of TOC are widely accepted as representing fair to medium quality of source rocks in the upslope area, and were not all higher than the lower TOC limit of 0.5% that has been determined for the main source rocks in the Mianyang–Changning Intracratonic Sag.

Maturity and Type of Organic Matter

Maturity is a parameter reflecting whether the source rock has evolved to the stage of oil or gas generation, and is the basis for evaluating its potential for hydrocarbon generation. Judgments of the thermal maturity of Paleozoic source rocks have long been controversial for the following reasons: 1) Higher plants appeared only after the Devonian (Li, 1994), and kerogen microscopic examination showed that organic matter in the source rocks was all derived from marine phytoplankton (algae) and bacteria, with no vitrinite. 2) The standards for conversion from R_b (bitumen reflectance) to R_o are usually different in different regions. 3) Under a high degree of thermal evolution, the rock pyrolysis method is easily affected by sample pollutants, and it is challenging to reliably measure T_{max}. 4) Analyzing the diagenetic evolution of clay minerals can be used to classify the stage of maturity, but cannot be used to quantitatively judge it. Due to the defects of each available method, we conservatively used 44 data items on rock pyrolysis T_{max} to identify the maturity of the source rocks of W207 Qiongzhusi Fm. The mature stage of black shale was divided into the following: R_o<0.5%, T_{max} <435°C was considered immature; 0.5% < R_o < 1.3%, 435°C < T_{max} < 475°C was considered mature; 1.3% < R_o < 2%, 475 °C < T_{max} < 500°C was considered highly mature; T_{max} > 500°C was considered to be in the stage of over-maturity, of which 2% < R_o < 3% was the early stage of over-maturity, and 3% < R_o < 4% was the late stage.

For highly mature source rocks of the Qiongzhusi Fm, the T_{max} measured by rock pyrolysis was less than 435°C, and could easily lead to the illusion of an immature source rock. This phenomenon occurred because the rate of conversion of Lower Cambrian source rocks is generally as high as 90%, resulting in a low S_2 value of the pyrolytic hydrocarbons. This makes the sample vulnerable to the "false peak" of pyrolysis generated by pollutants, and thus the peak temperature T_{max} of S_2 is low (Zhang et al., 2007). The values of T_{max} fluctuated between 293° and 612°C, indicating that most samples were subject to the peak value generated by the pyrolysis of the drilling fluid and solid asphalt, and could not represent their real maturity. S_1, S_2, and S_3 were very low, indicating that W207 has a small amount of residual hydrocarbons and poor capacity for hydrocarbon generation (**Figure 4**), and the source rock had entered the stage of high maturity. Samples with T_{max} greater than 475°C might have more accurately reflected the maturity (high-over maturity) of the source rock.

The organic carbon isotope ($\delta^{13}C$) can provide important information about the main types of organisms during the sedimentary period, and can reflect the main types of primitive organisms. It is an effective indicator of the types of organic matter in over-mature source rocks. The results showed that plankton was relatively abundant in lipids in the organic matter of different biological species. In addition, its high contribution led to lower values of organic carbon isotopes ($\delta^{13}C$), indicating the characteristics of sapropel type I kerogen (Huang, 1988; Tenger et al., 2004). The range of variation of organic carbon isotopes in the 44 samples of Qiongzhusi Fm was −34.95‰~ −30.44‰, with an average of −32.49‰. The range of variation of organic carbon isotopes at the bottom of Qiongzhusi Fm was −34.95‰~−32.60‰, with an average of −33.73%, that in the middle interval was −33.89‰~−30.80‰, with an average of −32.16‰, and that in the upper layer was −30.49‰~−30.44‰, with an average of −30.65‰, showing the characteristics of type I kerogen.

In combination with numerous algae macerals that are favorable for oil generation in the black rocks, the data suggest that both the LSQ and USQ might have made a significant contribution to the superabundant Lower Paleozoic petroleum resource over geological history (**Figure 5**). This is supported by numerous observations of asphaltene within the investigated black shale and the abundant bitumen-containing hydrocarbon reservoirs overlying them.

Effects of Paleoweathering and Terrigenous Detrital on Paleoproductivity

Paleoweathering

The WIP has been used to characterize the degree of weathering of silicate rocks (Srivastava et al., 2018). Owing to the abundant Si content of the earliest Cambrian Qiongzhusi Fm, the WIP provides the best option for quantifying the degree of paleoweathering and its effects on the formation of the black rocks in Qiongzhusi Fm. These were mainly the black shales in the $\epsilon_1 q^1$ and black siliceous rocks in the $\epsilon_1 q^{2\text{-}3}$. Furthermore, in light of bond strength, the individual mobilities of the most mobile major elements were considered when calculating the WIP (**Eqs. 1** and **2**), thus indicating that the WIP is widely applicable (Parker, 1970).

$$WIP = 100 \times \left\{ \left(\frac{2 \times Na_2O}{0.35} \right) + \left(\frac{MgO}{0.9} \right) + \left(\frac{2 \times K_2O}{0.25} \right) + \left(\frac{CaO^*}{0.7} \right) \right\} \quad (1)$$

$$CaO^* = CaO - CO_{2(calcite)} - (0.5 \times CO_2)_{(dolomite)} - \left[\frac{10}{3} \times P_2O_5 \right]_{(apatite)} \quad (2)$$

where the data in **Eq. 1** are as molar proportions of the oxides, and CaO* indicates the CaO content of silicate minerals,

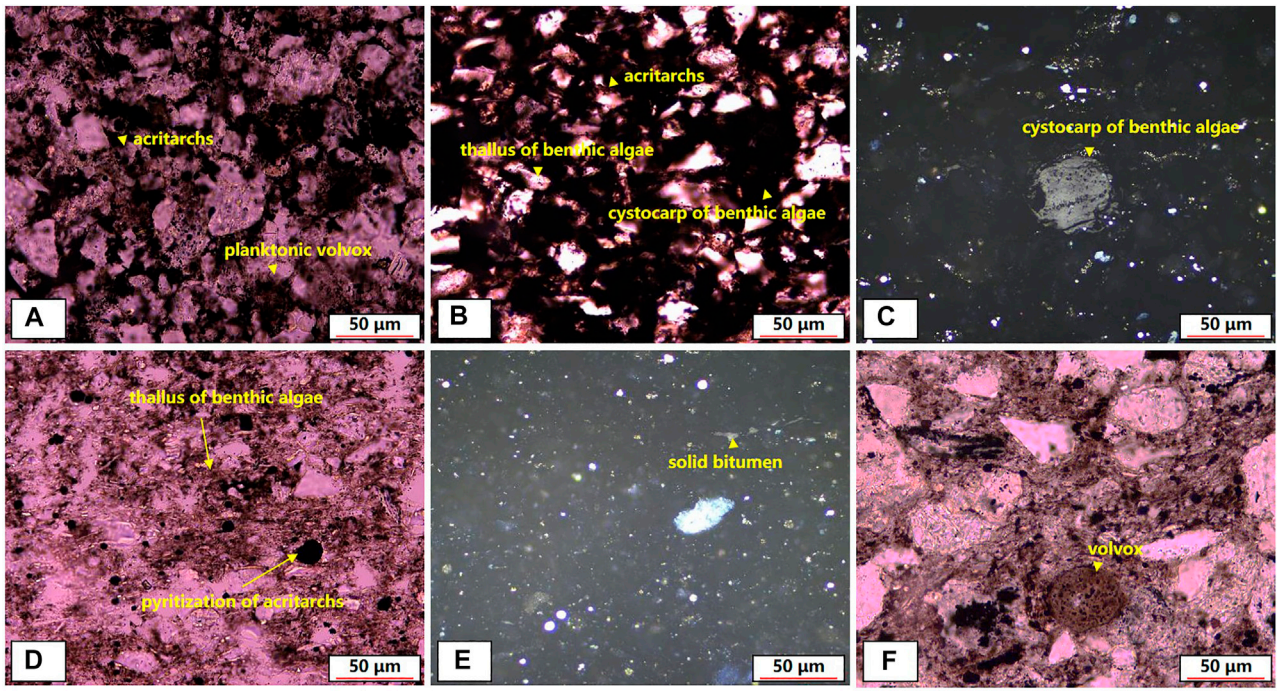

FIGURE 5 | Organic maceral characteristics of the Early Cambrian black strata, Qiongzhusi Fm, W-207 Well, NW Sichuan Basin. **(A–D)** relative abundant benthic algae, acritarchs **(E)** Numerous bitumen, and **(F)** abundant volvox.

excluding CaO bound in carbonates and silicates (Nesbitt and Young, 1982; He et al., 2020a).

The relatively low WIP values suggest more intense chemical weathering related to heavy rainfall and continental runoff under a warm and humid climate, whereas relatively high values indicate a relatively low degree of chemical weathering that relates to a cool and arid climate (Srivastava et al., 2018). **Table 2** shows that the WIP of each layer in W207 was relatively stable, ranging from 47.11% to 71.59% with an average of 59.38%. This shows that the paleoclimate of the upslope area was warm and humid in this period. The WIP of the Qiongzhusi Fm decreased gradually from the bottom to the top, indicating that weathering had gradually increased. Furthermore, these results indicate that the degree of weathering during the deposition of $\mathcal{E}_1q^{2\text{-}3}$ was much stronger than that during the deposition of $\mathcal{E}_1q^1$, thus suggesting that a higher abundance of terrigenous detrital matters was carried into the upper part in comparison with the lower part.

Terrigenous Detrital

The relative contributions of terrigenous detrital matter, as reflected by the Ti content of the sediments ((Terrigenous% $=(Ti_{sample}$ $Ti_{PAAS})\times100$); post-Archaean Australian shale (PAAS) with Ti = 5,995 ppm)) can also be used to provide insights into the degree of weathering. Relatively high values imply a stronger continental weathering (Taylor and Mclennan, 1985; Murray and Leinen, 1996; Li et al., 2017). The terrigenous value of siliceous shale samples from $\mathcal{E}_1q^3$ fluctuated between 70.08% and 73.48% (average of 71.90%), thus indicating strong continental weathering. The values ranged from 74.08% to 85.77% (average of 79.83%) within the black shale samples from $\mathcal{E}_1q^2$, showing stronger weathering. The terrigenous values were relatively low for shales from $\mathcal{E}_1q^1$, ranging from 57.98% to 86.97% (average of 73.21%), excluding samples W207–8 and W207-3 (37.09% and 45.78%, respectively) (**Table 2**). The values indicate much stronger weathering (from the top to the bottom) during the deposition of Qiongzhusi Fm, which is consistent with the results of the WIP.

Upwelling and Watermass Restriction

The Mo/TOC ratios of mudstone samples in well W207 ranged from 6.44% to 27.47% (mean, 14.37%). The Mo/TOC ratios in $\mathcal{E}_1q^2$ was 6.44–27.47 (mean 15.35), and those of $\mathcal{E}_1q^2$ and $\mathcal{E}_1q^3$ ranged from 6.90 to 26.41 (mean 11.79) and 8.27 to 20.92 (mean 12.92). Most of the samples of $\mathcal{E}_1q^1$ and $\mathcal{E}_1q^2$ were in the semi-restricted environment. The injection point of $\mathcal{E}_1q^2$ was above some of that of $\mathcal{E}_1q^1$, which indicates that the efficiency of circulation of the watermass was higher during this period of deposition, while it was closed during the deposition of $\mathcal{E}_1q^3$ in the upper part. The degree of limitation was close to that of the Framvaren Fjord. The Mo-TOC model shows that this was not a moderate restriction (**Figure 6A**).

The Mo_{EF}/U_{EF} ratios ranged from 1.51 to 9.38 (mean 4.24). Most of the samples in $\mathcal{E}_1q^1$ have high enrichment coefficients of Mo and U. Thus, the Mo_{EF}/U_{EF} ratio was high at 1.51–9.38 (mean 4.85). The Mo_{EF}/U_{EF} ratios of $\mathcal{E}_1q^2$ and $\mathcal{E}_1q^3$ are relatively low,

TABLE 2 | Analysis table of major and trace elements in Qiongzhusi Fm, W-207 Well.

Samples	SiO2/ %	Al/%	Fe/ %	Mn/ 10^{-2}%	P/ %	Zn/ ppm	V/ppm	Ba/ppm	Mo/ ppm	Ni/ ppm	Cu/ ppm	Cr/ ppm	Co/ ppm	Th/ ppm	U/ ppm	Mo_{EF}/ ppm	U_{EF}/ ppm	V_{EF}/ ppm	Ba_{bio}/ ppm	Ni/ Co	V/Cr	V/V + Ni	(P/ Al)/ 10^{-2}	U/ Th
W207-44	62.95	6.67	3.12	4.07	0.11	187.00	184.00	1,519.00	10.30	63.73	46.48	68.60	16.00	7.74	8.81	15.43	4.27	1.84	1,085.80	3.97	2.68	0.74	1.67	0.89
W207-43	57.02	8.18	4.34	4.69	0.10	151.00	197.00	1,581.00	6.67	56.84	49.68	97.40	19.40	10.80	6.71	8.16	2.65	1.61	1,049.55	2.94	2.02	0.78	1.17	0.67
W207-42	55.72	8.20	4.39	4.62	0.11	219.00	263.00	1945.00	7.69	68.67	69.66	103.00	20.50	11.00	8.90	9.39	3.50	2.14	1,412.31	3.36	2.55	0.79	1.30	1.20
W207-41	53.88	8.06	4.21	5.98	0.14	123.00	267.00	1,254.00	5.82	65.47	32.45	94.50	17.90	12.90	7.50	7.23	3.00	2.21	730.11	3.65	2.83	0.80	1.76	0.68
W207-40	55.93	8.68	4.41	4.82	0.13	141.00	257.00	1,356.00	5.59	71.24	40.53	99.20	19.20	13.00	7.32	6.45	2.72	1.97	791.94	3.71	2.59	0.78	1.52	0.72
W207-39	56.40	8.46	3.92	4.28	0.20	237.00	304.00	1,365.00	9.78	81.54	40.88	103.00	17.70	11.50	11.90	11.58	4.53	2.40	815.73	4.61	2.94	0.79	2.40	1.09
W207-38	67.72	6.72	2.45	4.14	0.13	76.40	98.40	859.00	2.48	31.85	23.15	74.70	10.00	11.20	4.54	3.70	2.18	0.98	422.33	3.18	1.32	0.76	1.97	0.39
W207-37	67.07	6.56	2.58	4.69	0.11	44.90	95.80	878.00	3.92	30.30	22.44	69.70	10.20	10.60	4.66	5.99	2.30	0.97	452.10	2.96	1.37	0.76	1.68	0.94
W207-36	66.75	6.93	2.71	4.21	0.12	98.40	94.40	945.00	4.07	33.40	21.30	75.70	10.90	11.60	5.75	5.87	2.68	0.91	494.99	3.06	1.25	0.74	1.76	0.53
W207-35	65.14	7.26	3.19	3.73	0.11	112.00	114.00	1,200.00	8.31	48.83	30.06	83.30	12.80	10.80	7.74	11.46	3.44	1.05	728.39	3.80	1.37	0.70	1.55	0.74
W207-34	61.32	7.53	4.02	4.01	0.09	96.50	155.00	1,376.00	15.90	65.44	46.93	96.90	15.60	11.80	12.90	21.11	5.52	1.37	886.75	4.18	1.59	0.70	1.23	1.14
W207-33	65.04	7.13	3.12	3.19	0.11	74.70	201.00	1,228.00	17.00	74.41	34.22	86.50	13.60	11.90	17.10	23.84	7.74	1.88	764.57	5.49	2.33	0.73	1.60	1.56
W207-32	62.75	7.47	3.51	2.99	0.13	142.00	455.00	1,158.00	15.60	111.05	35.39	99.50	15.80	12.00	15.70	20.90	6.80	4.06	672.98	7.05	4.57	0.80	1.73	1.90
W207-31	61.23	7.11	3.67	3.33	0.13	101.00	114.00	1,101.00	27.30	61.19	33.22	84.00	15.30	12.90	23.80	38.39	10.80	1.07	638.92	4.01	1.36	0.65	1.78	2.75
W207-30	58.30	6.72	4.43	5.98	0.09	44.30	100.00	955.00	15.20	49.71	40.23	80.70	14.80	11.50	8.40	22.63	4.04	1.00	518.47	3.35	1.25	0.67	1.29	0.76
W207-29	60.03	6.44	3.70	5.50	0.10	127.00	91.70	927.00	17.50	62.30	34.74	69.00	14.90	11.30	9.29	27.23	4.65	0.95	508.42	4.19	1.33	0.60	1.59	0.78
W207-28	61.96	7.40	3.82	3.06	0.11	92.20	137.00	1,007.00	13.40	69.42	35.52	88.00	17.40	12.30	9.78	18.13	4.27	1.24	526.21	3.99	1.56	0.66	1.46	0.76
W207-27	61.87	7.36	3.77	3.67	0.11	141.00	200.00	987.00	12.90	77.41	37.03	88.90	16.90	12.40	9.71	17.54	4.26	1.81	508.99	4.58	2.25	0.72	1.54	1.33
W207-26	59.80	6.76	3.43	6.45	0.10	118.00	143.00	888.00	9.90	61.62	30.91	79.00	15.50	10.80	6.03	14.65	2.88	1.41	448.75	3.98	1.81	0.70	1.41	0.52
W207-25	46.31	5.71	3.16	21.32	0.07	49.50	89.20	743.00	8.96	37.59	27.37	70.70	14.20	9.93	5.91	15.69	3.34	1.04	371.88	2.65	1.26	0.70	1.20	0.50
W207-24	61.75	7.07	3.76	4.07	0.10	53.30	107.00	906.00	9.84	39.32	34.87	84.10	15.80	12.00	6.55	13.92	2.99	1.01	446.46	2.49	1.28	0.73	1.38	0.58
W207-23	61.68	7.23	4.20	3.12	0.10	54.10	110.00	943.00	26.10	51.64	41.70	84.10	16.40	11.50	10.30	36.16	4.61	1.02	473.35	3.15	1.31	0.68	1.34	1.24
W207-22	66.27	5.26	1.56	7.47	0.11	27.80	58.30	1,070.00	1.16	14.49	13.71	49.40	5.31	8.33	2.37	2.21	1.46	0.74	728.29	2.73	1.18	0.80	2.12	0.21
W207-21	62.47	7.48	4.17	2.72	0.10	57.00	187.00	2,418.00	17.70	80.21	39.75	89.70	17.40	11.40	11.90	23.72	5.13	1.67	1931.88	4.61	2.09	0.70	1.30	0.99
W207-20	60.46	7.57	4.41	4.55	0.10	150.00	172.00	984.00	24.60	107.93	44.32	91.30	18.40	11.80	25.40	32.52	10.84	1.51	492.37	5.87	1.88	0.61	1.36	2.56
W207-19	62.85	7.49	3.96	2.99	0.10	190.00	793.00	954.00	22.50	101.50	43.35	98.40	17.50	11.50	16.80	30.02	7.24	7.06	467.26	5.79	8.07	0.89	1.37	1.56
W207-18	45.21	5.21	4.38	27.98	0.09	48.30	191.00	689.00	9.34	60.94	24.08	69.70	14.00	7.31	7.99	17.95	4.95	2.45	350.83	4.36	2.75	0.76	1.70	0.64
W207-17	62.11	7.63	4.08	2.78	0.11	152.00	727.00	918.00	21.50	95.29	40.59	98.90	17.50	12.90	16.70	28.24	7.08	6.36	422.62	5.45	7.35	0.88	1.49	1.35
W207-16	59.62	8.13	4.94	2.85	0.11	103.00	557.00	960.00	17.20	115.25	45.72	112.00	20.80	11.90	15.20	21.13	6.03	4.57	432.09	5.54	4.96	0.83	1.40	1.35
W207-15	61.67	7.62	3.73	2.58	0.12	52.40	125.00	1,159.00	29.50	64.15	42.58	86.50	16.30	11.10	14.90	38.80	6.33	1.09	664.00	3.93	1.44	0.66	1.55	1.29
W207-14	59.53	6.80	3.93	3.53	0.11	299.00	895.00	1,121.00	24.60	154.28	52.58	91.60	15.40	8.64	15.80	36.22	7.50	8.78	679.28	10.01	9.76	0.85	1.56	1.22
W207-13	55.89	5.76	3.35	5.16	0.10	110.00	169.00	1,035.00	35.50	122.48	42.91	64.50	14.70	8.27	24.20	61.77	13.56	1.96	660.96	8.34	2.63	0.58	1.80	2.01
W207-12	60.87	7.17	4.04	2.38	0.09	42.10	131.00	1,183.00	33.50	76.70	56.23	85.00	18.40	11.00	17.20	46.79	7.74	1.22	716.96	4.17	1.54	0.63	1.30	1.44
W207-11	58.94	7.42	3.68	3.26	0.09	47.80	123.00	1,221.00	25.30	80.31	41.39	85.40	17.30	11.30	12.10	34.20	5.27	1.10	739.21	4.65	1.44	0.61	1.25	1.03
W207-10	59.52	6.99	3.30	3.67	0.09	48.20	109.00	1,167.00	25.50	89.35	38.97	85.00	21.30	10.50	8.42	36.51	3.89	1.04	712.72	4.19	1.28	0.55	1.28	0.78
W207-09	60.49	7.18	3.35	3.12	0.08	49.70	123.00	1,201.00	22.30	79.68	44.48	81.40	19.60	10.80	9.88	31.10	4.44	1.14	734.69	4.07	1.51	0.61	1.18	0.85
W207-08	56.21	4.61	1.45	7.47	0.07	20.30	42.70	1,035.00	1.99	20.48	10.89	31.90	6.20	4.93	3.92	4.32	2.75	0.62	735.62	3.30	1.34	0.68	1.57	0.37
W207-07	58.08	6.97	5.13	2.58	0.09	120.00	205.00	1,347.00	38.30	126.69	59.49	88.70	16.70	11.70	24.00	54.98	11.11	1.96	894.30	7.58	2.31	0.62	1.24	2.15
W207-06	58.82	7.18	4.61	2.38	0.09	132.00	226.00	1,448.00	29.90	82.03	58.62	88.90	16.80	10.90	22.10	41.66	9.92	2.10	981.75	4.90	2.54	0.73	1.22	1.93
W207-05	62.54	7.11	3.27	2.31	0.11	115.00	985.00	1,445.00	20.10	104.55	53.87	98.80	16.60	10.20	19.10	28.27	8.69	9.24	982.98	6.30	9.97	0.90	1.49	1.47
W207-04	63.01	6.93	3.04	2.38	0.08	881.00	1,245.00	1,550.00	20.00	98.46	88.11	119.00	15.10	11.00	13.50	28.85	6.31	11.99	1,100.02	6.53	10.46	0.93	1.22	1.05
W207-03	43.28	4.67	3.00	12.97	0.06	31.60	213.00	1,317.00	24.60	53.78	37.51	60.90	11.30	7.40	16.90	52.71	11.66	3.04	1,013.84	4.75	3.49	0.80	1.38	1.53
W207-02	59.96	6.79	3.43	2.65	0.08	586.00	923.00	1,627.00	60.10	183.09	59.43	91.00	20.70	10.10	30.00	88.59	14.28	9.07	1,186.20	8.87	10.14	0.83	1.21	2.77
W207-01	61.15	6.47	2.98	2.92	0.09	86.20	967.00	1972.00	55.00	209.46	45.40	85.90	17.90	9.87	27.70	85.05	13.81	9.97	1,551.74	11.69	11.26	0.82	1.44	3.58
PAAS	62.80	10.01	5.05	7.47	0.07	85.00	150.00	650.00	1.00	55.00	50.00	110.00	23.00	14.60	3.10	—	—	—	—					

ranging from 1.69 to 5.60 (mean 3.22) and 2.37 to 3.62 (mean 2.79). The most samples from $\epsilon_1 q^2$ and $\epsilon_1 q^3$ is 0.3–1 times the seawater. Under the enhancement of seawater reduction conditions, the rates of uptake of Mo that substantially exceed those of U, resulting in a progressive increase in sediment Mo_{EF}/U_{EF} ratios of most samples in $\epsilon_1 q^1$ at the bottom to more than 1 times the seawater. However, it is far lower than the ratio of Mo affected by the adsorption of manganese and iron particle carriers (Mo/U ratio is 3–10 times). At higher enrichment coefficients, Mo_{EF}/U_{EF} did not decrease further, which indicates a connection between the ocean and the open sea in this area during the deposition of the Qiongzhusi Fm. The circulation efficiency of watermasses was high, and this was an unrestricted marine environment (**Figure 6B**).

The contents of Co and Mn are generally low in an upwelling setting due to the loss of Co and Mn in the secondary oxidation environment. However, watermasses with a higher degree of restriction seawater show higher Co and Mn contents due to the external input (Sweere et al., 2016). For example, the hydrologic characteristics of the upwelling setting in Namibia, Peru, and Gulf of California are low $Co_{EF} \times Mn_{EF}$ (<0.5). At the same time, the limited Black Sea Basin has a higher $Co_{EF} \times Mn_{EF}$ (> 2) (Sweere et al., 2016). $Co_{EF} \times Mn_{EF}$ of $\epsilon_1 q^1$ is 0.42–8.42 (average 1.25); $Co_{EF} \times Mn_{EF}$ of $\epsilon_1 q^2$ is 0.49–1.14 (average value is 0.63); $Co_{EF} \times Mn_{EF}$ of $\epsilon_1 q^3$ is 0.62–0.96 (mean 0.79). As shown by $Co_{EF} \times Mn_{EF}$, the values of most samples ranged from 0.5 to 2, and their seawater environment could not be accurately distinguished. These samples might have been affected by unstable seasonal rises in the ocean current. Combined with the above, we think that in the sedimentary period, the ocean in the upslope area was related to the open sea. The efficiency of circulation of the watermasses was high, showing a moderately restricted marine environment (**Figure 6C**).

Redox Conditions

Effect on $\delta^{13}C_{org}$

The change in $\delta^{13}C_{org}$ can reflect changes in the degree of burial of organic matter, and depends on the change in marine primary productivity and the degree of preservation of organic matter in anoxic water (Goldberg et al., 2007; Schoepfer et al., 2015; Zhang et al., 2018). The positive values of $\delta^{13}C_{org}$ positive for W207 and the upward decrease in its TOC content indicate that conditions for the preservation of organic matter had worsened, and the sedimentary environment had gradually transitioned from anoxic to oxidic. This was compared with the data on $\delta^{13}C_{org}$ from the W207 well and the Songlin Section (Chen et al., 2006) in upslope, the Songtao Section in the downslope, and the Longbizui Section in the deep-water basin. The values of $\delta^{13}C_{org}$ of the Songtao Section in the downslope (deep-water shelf facies) were −34.7‰~−29.3‰ (mean −31.89‰), and that of the Longbizui Section was −36.5‰~−33.5‰ (mean −34.48‰), similar to those of the Weiyuan and Songlin areas. This shows that the value of $\delta^{13}C_{org}$ was significantly higher than that in sedimentary areas with deep water characteristics. Negative values of $\delta^{13}C_{org}$ were noted at the bottom of the middle and upper Yangtze, which was a widespread transgression event of the Yangtze Plate in the Early Cambrian (Guo et al., 2013; Wang et al., 2015). In this context, the

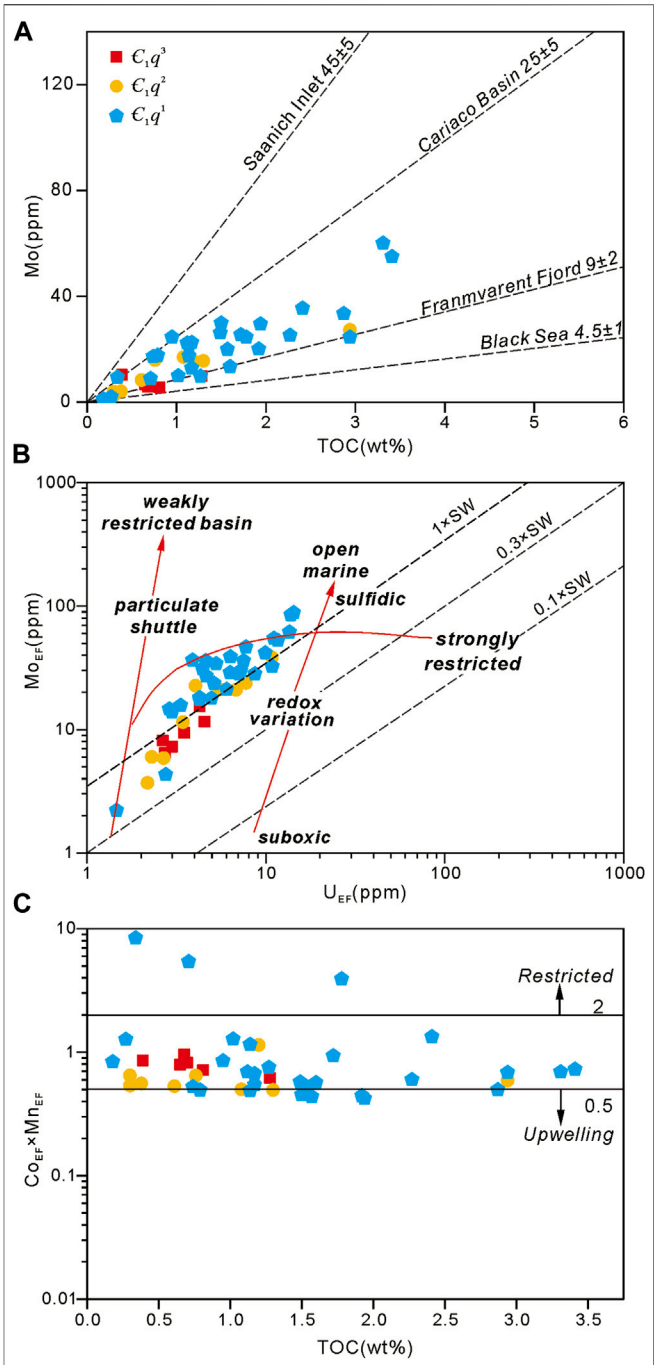

FIGURE 6 | (A) For the Early Cambrian in the Qiongzhusi Fm, W207 Well, upslope area of Yangtze Platform, compared with generalized patterns of sedimentary Mo-TOC covariation associated with deepwater renewal in silled anxic basins (eg., Black Sea, Framvaren Fjord, Cariaco Basin and Saanich Inlet) ((Algeo and Lyons, 2006). **(B)** Euxinic conditions indicated by U_{EF} vs. Mo_{EF} during the deposition of the early Cambrian Qiongzhusi Fm, SW Sichuan Basin. Dotted lines show MoEF/UEF ratios equal to the seawater (SW) value (i.e., 1 × SW) and fractions thereof (0.3 × SW, and 0.1 × SW) (Algeo and Tribovillard, 2009). **(C)** Crossplots of $Co_{EF} \times Mn_{EF}$ vs. TOC for the Qiongzhusi Fm in the W207 Well. The model data is from Sweere et al. (2016). $\epsilon_1 q^{1,2,3}$: first, second and third member of the Qiongzhusi Fm.

Yangtze Platform was in an anoxic environment caused by global transgression in this period. After the regression, the Weiyuan area on the upslope entered the oxidation state earlier. Then, such deep-water areas as the intracratonic sag and deep-water basin gradually tended toward oxidation.

A certain correlation was noted between changes in the redox environment and values of $\delta^{13}C_{org}$ in different areas of the Yangtze Platform. Although the trend was one of increase, there was some variation in $\delta^{13}C_{org}$ across the profiles. The Weiyuan and Songlin areas on the upslope area which their $\delta^{13}C_{org}$ records are similar, and $\delta^{13}C_{org}$ is higher than the deepwater basin area. The difference of $\delta^{13}C_{org}$ composition, redox environment and TOC content can be better explained. With the gradual oxidation of the water environment in Weiyuan and Songtao areas, organic matter is gradually degraded, resulting in $\delta^{13}C_{org}$ value beginning to increase first. The deep-water area is still in a continuous anoxic environment, with a large amount of organic matter preserved and the input of chemoautotrophic biomass to organic matter (Goldberg et al., 2007), with negative $\delta^{13}C_{org}$ excursion. It can be seen that the difference in $\delta^{13}C_{org}$ in different areas of the Yangtze Platform reflects the difference in organic matter preservation caused by the change of marine redox environment.

Effect on Elemental Parameters

The ratios of the redox-sensitive elements V/Cr, U/TH, and C_{org}/P are important indicators of the redox environment of paleo-oceans (Och et al., 2013; Pi et al., 2013; Jin et al., 2020; Zhao et al., 2020). The phosphorus cycle in sediments, measured in terms of the C_{org}/p value, is often controlled by redox conditions. Under oxidation conditions, phosphorus P element is generally adsorbed by iron hydroxide and stored in sediments (Kraal et al., 2010; Westermann et al., 2013). In anoxic environments, iron hydroxide in sediments dissolves, resulting in the release of adsorbed phosphorus (März et al., 2008). $C_{org}/p < 50$ indicates an oxic marine environment, $50 > C_{org}/p > 100$ indicates a secondary oxidation environment, $C_{org}/p > 100$ indicates an anoxic environment (Algeo and Ingall, 2007).

The V/Cr, Ni/Co, U/TH, and C_{org}/P ratios of the Qiongzhusi Fm had similar vertical variations in the W207 Well (**Figure 7**). Generally high U/Th and V/Cr ratios were obtained at the bottom of the Qiongzhusi Fm, ranging from 0.80 to 2.98 (mean 1.77) and 1.28–11.26 (mean 4.74). This indicates that the sedimentary environment in this period generally ranged from one of secondary oxidation to anoxia. After this, it transitioned to a short oxidation period; but then the water returned to an anoxic state. The gray mudstone section in the lower part of the Qiongzhusi Fm (near 3,180 m) had high U/Th (1.09–1.46, mean1.28) and V/Cr values (2.75–8.07, mean 5.78), indicating that the anoxic sedimentary environment had been restored to a certain extent. Subsequently, the U/Th and V/Cr ratios decreased and gradually stabilized, indicating that the sedimentary environment had changed from anoxic to one of oxidation. During the middle deposition stage of the Qiongzhusi Fm (around 3,130 m), the sedimentary environment changed

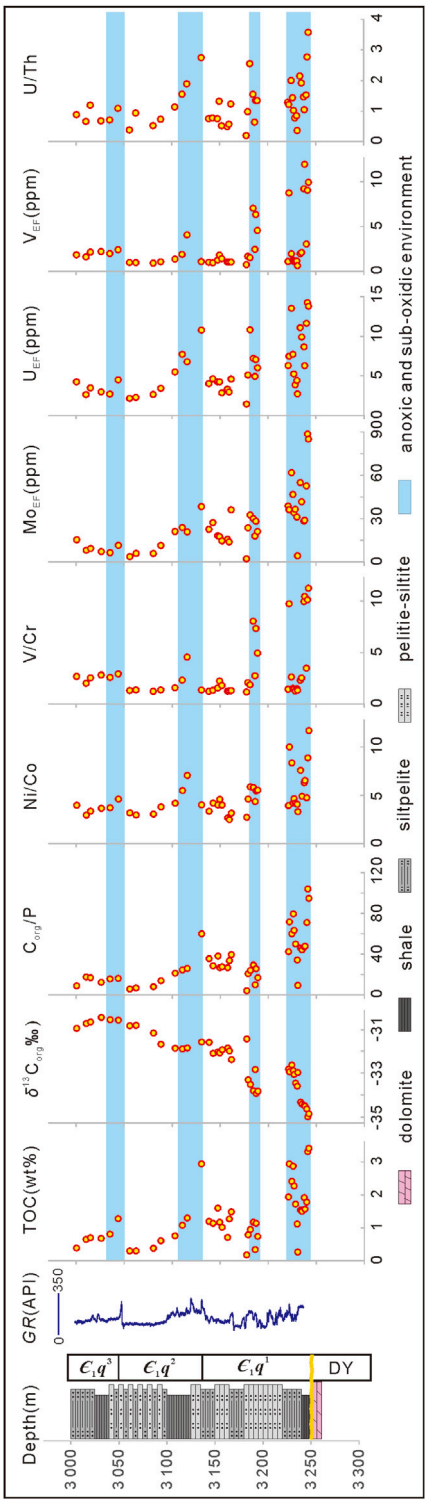

FIGURE 7 | Characteristics of the paleo-marine environment (redox parameters) of the Qiongzhusi Fm, W-207 Well. $\epsilon_1q^{1,\ 2,3}$: first, second and third member of Qiongzhusi Fm.

again. The U/Th and V/Cr ratios reached 1.84 and 4.57, respectively, and the water was in an anoxic state once again, but finally transitioned to the highest oxidation environment. Values of U/Th and V/Cr of samples at the top of the Qiongzhusi Fm were less than 1.25 and 4.25, respectively, indicating that the marine environment had been in a fairly stable oxidation to secondary oxidation state during this period (Jones and Manning, 1994).

The value of C_{org}/P of samples at the bottom of Qiongzhusi Fm was 9.57–104.02 (mean 57.71), indicating that it was deposited in an environment of partial anoxic reduction. The value of C_{org}/P of the remaining lower section (middle and upper part) was low, with a range of 4.12–39.62 (except samples at 3,130.65 m), indicating a relatively oxidized environment. C_{org}/P for samples at 3,130.65 m was 60, indicating that the oxygen content in seawater was relatively low during this period. This is consistent with the results indicated by the V/Cr and U/Th ratios.

The analyses of the above indices (element ratio, enrichment coefficient, and C_{org}/P) shows that the sedimentary environment of Qiongzhusi Fm has undergone an evolution of the form anoxic–oxidation–anoxic–secondary oxidation. During the stage of earlier deposition of the Qiongzhusi Fm, the marine environment was strongly anoxic, and then gradually tended to oxidize. During middle deposition, the sedimentary environment briefly changed to anoxic and then transitioned to an oxidation environment once again. At the end of deposition, the ocean in the upslope area, west of the intracratonic sag, was generally in an oxidation–secondary oxidation environment. The results show prominent anoxic watermass in the earlier sedimentary period of the Qiongzhusi Fm, which might be related to transgressive events in the same period. Then, the marine environment gradually transitioned to oxidation with regression.

Paleoproductivity

In the Early Cambrian, the marine ecosystem was relatively singular. Primary productivity mainly depended on the carbon-generating capacity of phytoplankton on the surface of seawater, and their prosperity depended on the abundance of nutrient elements in the ocean. In addition, the genesis, enrichment, and preservation of biogenic barium were closely related to the degradation of organic matter. When there was no strong sulfate reduction, the increase in biological productivity was related to the increase in elemental Ba content in organic-rich sediments. Therefore, biogenic Ba is an effective indicator of paleoproductivity (Stroobants et al., 1991; Von Breymann et al., 1992).

We found that such parameters of productivity as Cu/Al, Zn/Al, Ni/Al, and Ba_{bio} had high values at the bottom and in the middle of the Qiongzhusi Fm. At the same time, the remaining lithologic sections had low values (**Figure 8**), indicating that the western ocean of the Upper Yangtze Platform had a certain productivity in the early sedimentary stage of the Qiongzhusi Fm. With the evolution of the sedimentary stage, its productivity gradually decreased. The two sets of strata with high TOC values at the bottom and middle of the Qiongzhusi Fm correspond to the productivity indicated by the above parameters. During the period of a slight increase in TOC content at the top of the Qiongzhusi Fm (3,050 m), the vertical trend of change in the parameters of productivity, such as Ni/Al, Cu/Al, Zn/Al, and Ba_{bio}, also indicated that productivity had picked up in this period. Therefore, changes in productivity might have affected the accumulation of organic matter in the mudstone of the Qiongzhusi Fm.

Mechanism of Organic Matter Enrichment in Upslope Area

Main Factors Controlling the Enrichment of Organic Matter

Terrigenous input, sedimentary hydrodynamics, redox conditions, and productivity are closely related to the enrichment of organic matter. Our analysis shows that the WIP of the Qiongzhusi Fm was relatively stable. A warm and humid paleoclimate during the sedimentary period of the Qiongzhusi Fm was conducive to biological activities and a rich source of organic matter. However, there was no significant correlation between the WIP and the TOC (**Figure 9A**); we think that the paleoclimate was not the main factor controlling the enrichment of organic matter in the Qiongzhusi Fm in the upslope area. In addition, the map of intersection of indicators of terrigenous input (Terrigenous, Ti/Al) and TOC also show no significant correlation between the terrigenous input and the enrichment of organic matter (**Figures 9B,C**). Although the Weiyuan area is located on an upslope on the west side of the intracratonic sag, a certain amount of terrigenous input (increasing gradually from bottom to top) caused a decrease in organic matter content. Therefore, the input of terrigenous clasts on the western margin of the Yangtze Platform might not have been conducive to the enrichment of organic matter of the Qiongzhusi Fm.

Comprehensive Mo/TOC, $Co_{EF} \times Mn_{EF}$ and Cd/Mo hydrodynamic condition indexes. In particular, Cd is related to algal productivity. For the Black Sea with a strong restriction, the primary productivity and organic matter accumulation rate are very low. The Cd/Mo ratio of the sediment was close to that of seawater. The relatively high-level primary productivity might have led to the more effective entry of Cd into deeper seawater and sediments. Compared with Mo, a slight enrichment of Cd was observed. Sweere et al. (2016) summarized the differences in Cd/Mo in different restriction basins, and limited the boundary between productivity and preservation conditions, the two factors controlling the enrichment of organic matter, to a Cd/Mo value of 0.1. This is an empirical value; if Cd/Mo is greater than 0.1, the enrichment of organic matter in sediments is mainly controlled by productivity, and if Cd/Mo is less than 0.1, the enrichment is mainly controlled by preservation conditions. The overall variation in Cd/Mo in the W207 Well was between 0.002 and 0.072, with an average value of 0.013, indicating that preservation conditions mainly controlled the enrichment of organic matter of sediments in this area.

The oxygen content in seawater directly determines whether the organic matter can be well preserved in sediments for large-scale enrichment. A relatively restricted sedimentary environment, a certain extent of upwelling, and a widely developed anoxic

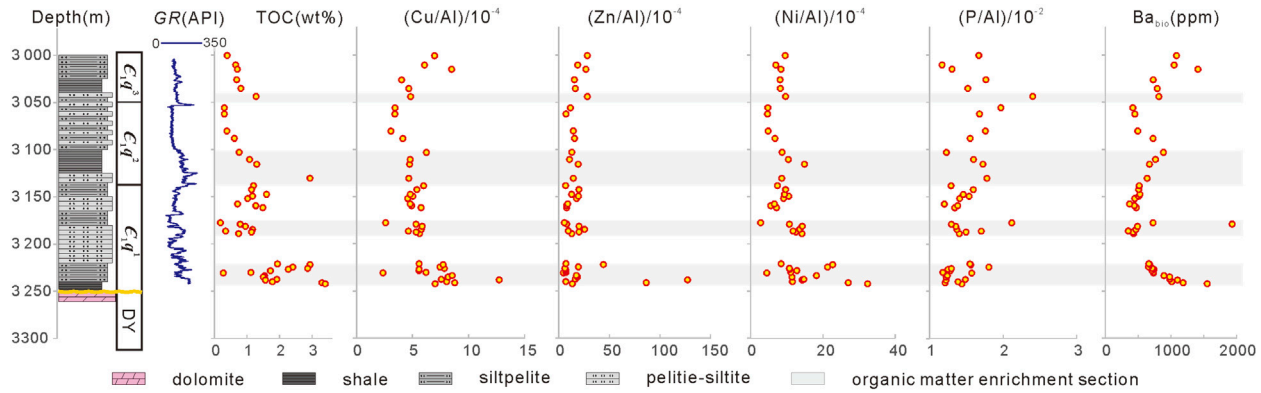

FIGURE 8 | Characteristics of paleo-ocean productivity parameters of the Qiongzhusi Fm, W-207 Well. $\epsilon_1 q^{1,2,3}$: first, second and third member of Qiongzhusi Fm.

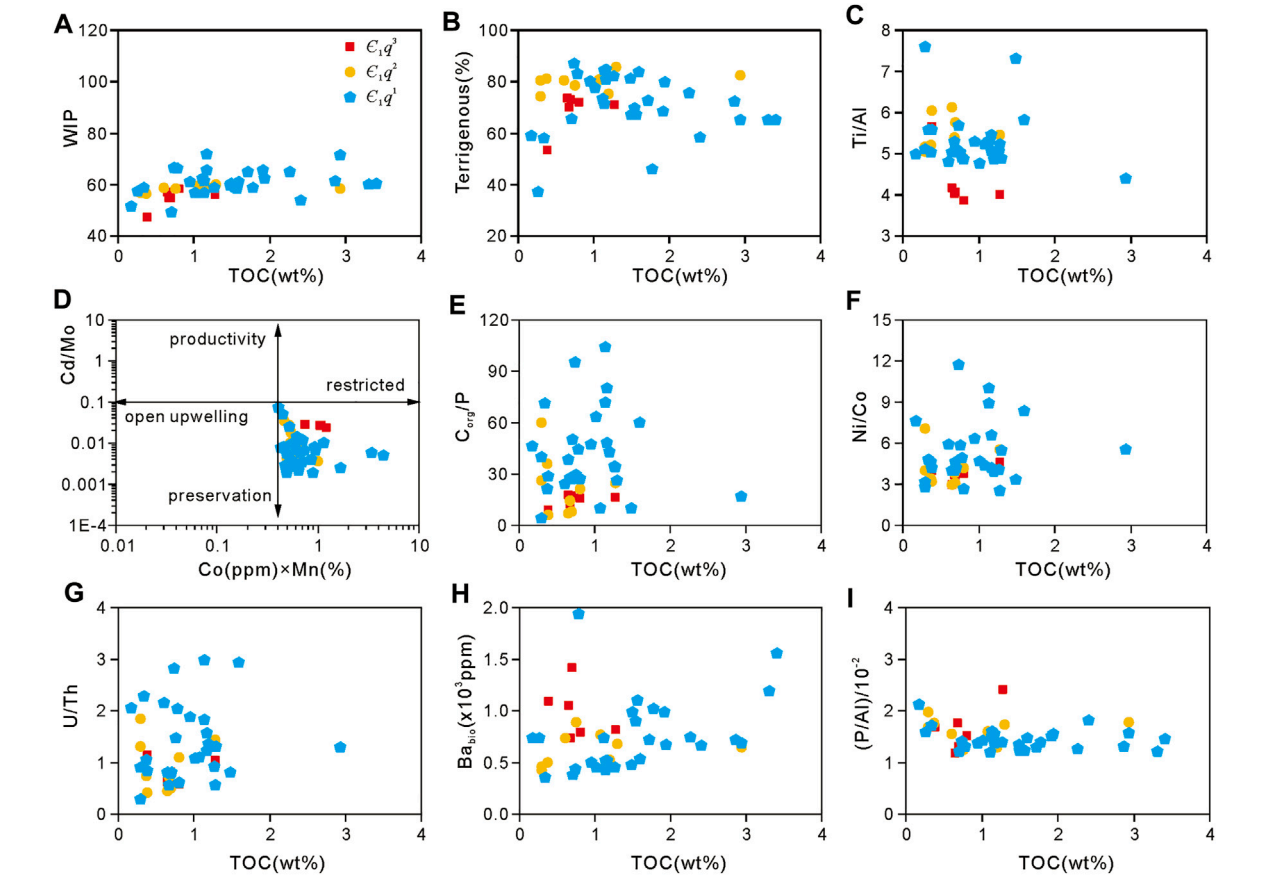

FIGURE 9 | Cross-plots indicating the organic matter enrichment mechanism of the Early Cambrian Qiongzhusi Fm, W207 Well, SW Sichuan Basin. **(A-B)** paleoweathering and terrigenous detrital index vs. TOC (organic matter enrichment). **(C-D)** hydrodynamic index vs. TOC. **(E-G)** redox index vs. TOC. **(H-I)** paleoproductivity index vs. TOC. WIP: weathering index of Parker (Parker, 1970); Terrigenous: Ti content of sediments; Babio: biogenic Ba; TOC: total organic carbon; $\epsilon_1 q^{1,2,3}$: first, second and third member of Qiongzhusi Fm.

environment promote the preservation of organic matter and the enrichment of redox-sensitive elements. A strong positive correlation was noted between parameters of the redox index (such as C_{org}/P, Ni/Co, and U/Th) and TOC in the Qiongzhusi Fm, W207 (**Figures 9E–G**). From an anoxic to an oxic environment, the oxidation–reduction conditions during the deposition of the

Qiongzhusi Fm changed from bottom to top in the Weiyuan area. The anoxic interval in $\epsilon_1 q^1$ was the most enriching in organic matter. The redox conditions of the sedimentary environment were the key factors controlling the preservation and enrichment of organic matter in the upslope area, west of the Mianyang–Changning Intracratonic Sag.

The primary productivity of surface seawater is an important source of organic matter in the shale. Enriching organic matter also requires high biological productivity to provide organic carbon as a material guarantee. However, such paleoproductivity indicators as Zn, P/Al, and Ba_{bio} were weakly correlation with the TOC (R^2Zn = 0.0726, R^2p = 0.0451, R^2Ba_{bio} = 0.0575) in the Qiongzhusi Fm, W207. A certain positive correlation was noted between P/Al and TOC in $\epsilon_1 q^1$ and $\epsilon_1 q^2$, and the ocean in the upslope area had a certain productivity (**Figures 9H–I**). With continuous sedimentary evolution, the productivity gradually decreased. P/Al and the TOC changed to a negative correlation in $\epsilon_1 q^2$, possibly due to the influence of changes in seawater redox conditions on the increase in phosphorus content. It reflects a certain productivity in this period. However, its strength of control over the enrichment of organic matter for shale was secondary.

Enrichment of Organic Matter During the Deposition of Qiongzhusi Fm in the Upslope Area

The process of enrichment of organic matter in Qiongzhusi Fm in the upslope area, west of the Mianyang–Changning Intracratonic Sag, is the key issue for assessing the potential for shale gas in the Southwest Sichuan Basin. Higher productivity can provide rich sources of organic matter and an anoxic environment can provide good preservation conditions (Zhang et al., 2018). Under the background of large-scale transgression during the early stage of deposition of the Qiongzhusi Fm (Feng et al., 2014; Zhai et al., 2016; Zhao et al., 2020; Fan et al., 2021), the Leshan–Weiyuan slope in the west side of the Mianyang–Changning Intracratonic Sag was connected to the open sea. Accompanied by a certain degree of upwelling in the sea water and rich nutrients imported from the deep seawater, this rendered productivity high during the early deposition of the Qiongzhusi Fm. Meanwhile, the widely developed anoxic environment further promoted the preservation of a large amount of organic matter and the enrichment of redox-sensitive elements in the lower layer of the Qiongzhusi Fm. With the regression of the sea, the sedimentary environment gradually transitioned to one of oxidation, with conditions for the preservation of organic matter gradually deteriorating.

During the middle deposition stage of the Qiongzhusi Fm, the sea level in the study area rose again. The sedimentary environment returned to a relatively anoxic state, and became rich in organic matter once again. The two sets of sedimentary sections under an anoxic paleo-ocean environment showed significant enrichment in organic matter, indicated by the TOC content. As the coupling between TOC and the redox index is better than that between it and the paleoproductivity index, a significant enrichment of organic matter (abnormally high TOC content) occurred during the depositon of $\epsilon_1 q^3$ (3,130.65 m). However, the change in productivity, reflected by such productivity indices as Cu/Al, Zn/Al, and Ba_{bio}, was not prominent. Therefore, under the condition that the productivity did not change significantly, the anoxic condition created a better preservation environment for organic matter.

Ultimately, the change in sea level controlled the redox conditions, productivity, and thus the accumulation of organic matter during the formation of Earlier Cambrian black shale in the upslope, Upper Yangtze Platform (**Figure 10**). Although productivity affected the enrichment of organic matter in the black strata to a certain extent, it was not the main factor controlling it in the upslope area. A good coupling between redox environmental indicators and the TOC shows that the mechanism of enrichment of organic matter during the

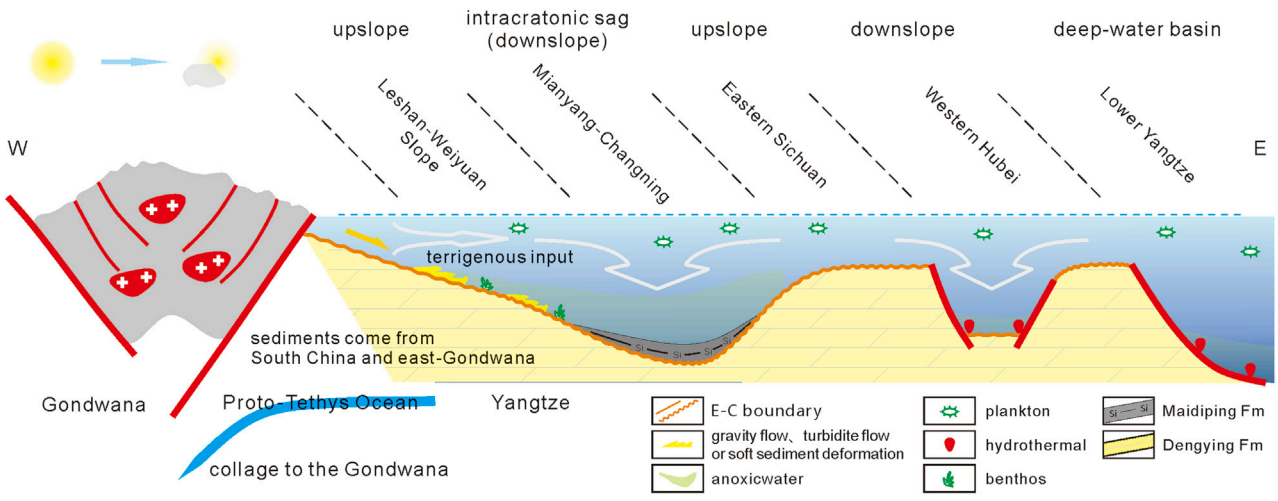

FIGURE 10 | Sedimentary paleo-ocean environment and productivity model of the Qiongzhusi Fm in the upslope area.

formation of Qiongzhusi Fm black shale in the Earlier Cambrian was controlled more by paleo-ocean redox conditions, which ultimately determined the content of organic matter.

CONCLUSION

1) Interactive conversion cycles developed between multiple deep-water and shallow-water shelves under the control of the sea level rise in the upslope area, but the shallow-water shelf facies mainly developed. Typical slope turbidite- (fan) and gravity flow-induced deposits developed. The wells in the upslope area represented by the Weiyuan area did not have long-term deep-water sedimentary conditions, and the layer of organic, rich, black shale was thin.
2) The results of organic geochemistry showed that organic matter in the Qiongzhusi Fm was mainly type I kerogen, with a high degree of thermal evolution, little amounts of residual hydrocarbons, and low capacity for hydrocarbon generation.
3) The redox indices (U/Th, C_{org}/P, and U_{EF}) showed that the sedimentary environment in the Early Cambrian in the upslope area underwent the anoxic oxidation–anoxic-secondary oxidation evolution; the marine environment was moderately restricted, with a certain degree of upwelling.
4) Change in the sea level controlled the redox conditions and productivity, and thus the enrichment of organic matter of the Qiongzhusi Fm. Productivity affected the accumulation of organic matter to a certain extent but was not the main factor controlling it. Redox conditions are key to the formation of organic matter.

DATA AVAILABILITY STATEMENT

The original contributions presented in the study are included in the article/Supplementary Material, further inquiries can be directed to the corresponding author.

AUTHOR CONTRIBUTIONS

LZ: Data Curation; Writing; Methodology; Investigation SL: Conceptualization; Project administration; Funding acquisition GL: Investigation; Formal analysis MZ: Validation; Methodology; Funding acquisition XL: Data Curation; Writing; Methodology; Investigation JL: Formal analysis

REFERENCES

Algeo, T. J., and Ingall, E. (2007). Sedimentary Corg:P Ratios, Paleocean Ventilation, and Phanerozoic Atmospheric pO2. *Palaeogeogr. Palaeoclimatol. Palaeoecol.* 256, 130–155. doi:10.1016/j.palaeo.2007.02.029

Algeo, T. J., and Lyons, T. W. (2006). Mo-Total Organic Carbon Covariation in Modern Anoxic marine Environments: Implications for Analysis of Paleoredox and Paleohydrographic Conditions. *Paleoceanography* 21. doi:10.1029/2004PA001112

Algeo, T. J., and Tribovillard, N. (2009). Environmental Analysis of Paleo-Oceanographic Systems Base on Molybdenum–Uranium Covariation. *J. Chem. Geol.* 268 (3), 211–225. doi:10.1016/j.chemgeo.2009.09.001

Algeo, T., Shen, Y., Zhang, T., Lyons, T., Bates, S., Rowe, H., et al. (2008). Association of ^{34}S-Depleted Pyrite Layers with Negative Carbonate δ^{13}C Excursions at the Permian-Triassic Boundary: Evidence for Upwelling of Sulfidic Deep-Ocean Water Masses. *J. Geochem. Geophy. Geosy.* 9 (4), 5–6. doi:10.1029/2007gc001823

Babechuk, M. G., Widdowson, M., and Kamber, B. S. (2014). Quantifying Chemical Weathering Intensity and Trace Element Release from Two Contrasting basalt Profiles, Deccan Traps, India. *Chem. Geology.* 363, 56–75. doi:10.1016/j.chemgeo.2013.10.027

Baturin, G. N. (2011). Geochemistry of Sapropel in the Black Sea. *Geochem. Int.* 49 (5), 531–535. doi:10.1134/s0016702911050028

Brumsack, H.-J. (1989). Geochemistry of Recent TOC-Rich Sediments from the Gulf of California and the Black Sea. *Geol. Rundsch* 78 (3), 851–882. doi:10.1007/bf01829327

Bush, A. M., Bambach, R. K., and Daley, G. M. (2007). Changes in Theoretical Ecospace Utilization in Marine Fossil Assemblages between the Mid-paleozoic and Late Cenozoic. *Paleobiology* 33 (1), 76–97. doi:10.1666/06013.1

Chang, C., Hu, W., Fu, Q., Cao, J., Wang, X., and Yao, S. (2016). Characterization of Trace Elements and Carbon Isotopes across the Ediacaran-Cambrian Boundary in Anhui Province, South China: Implications for Stratigraphy and Paleoenvironment Reconstruction. *J. Asian Earth Sci.* 125, 58–70. doi:10.1016/j.jseaes.2016.05.014

Chen, L., Zhong, H., Hu, R. Z., and Xiao, J. F. (2006). Composition of Organic Carbon Isotope of Early Cambrian Black Shale in the Xiang-Qian Area and its Significances. J. *J. Mineralogy Petrol.* 26, 81–85. doi:10.1109/TPSD.2006.5507455

Chen, Q., Sun, M., Long, X., Zhao, G., Wang, J., Yu, Y., et al. (2018). Provenance Study for the Paleozoic Sedimentary Rocks from the West Yangtze Block: Constraint on Possible Link of South China to the Gondwana Supercontinent Reconstruction. *Precambr. Res.* 309, 271–289. doi:10.1016/j.precamres.2017.01.022

Craig, P., Chevrier, V., Sayyed, M. R. G., and Islam, R. (2017). Spectral Analysis of Deccan Intrabasaltic Bole Beds: Implications for the Formation and Alteration of Phyllosilicates on Mars. *Planet. Space Sci.* 135, 55–63. doi:10.1016/j.pss.2016.11.008

Ding, Y., Li, Z., Liu, S., Song, J., Zhou, X., Sun, W., et al. (2021). Sequence Stratigraphy and Tectono-Depositional Evolution of A Late Ediacaran Epeiric Platform in the Upper Yangtze Area, South China. *Precambrian Res.* 354, 106077. doi:10.1016/j.precamres.2020.106077

Fan, H., Deng, H., Fum, M., Liu, S., Yu, H., and Li, Y. (2021). Sedimentary Characteristics of the Lower Cambrian Qiongzhusi Formation in the Sichuan Basin and its Response to Construction. *J. Acta Sedimentol. Sin.* 39 (04), 1004–1019. doi:10.14027/j.issn.1000-0550.2020.041

Fedo, C. M., Wayne Nesbitt, H., and Young, G. M. (1995). Unraveling the Effects of Potassium Metasomatism in Sedimentary Rocks and Paleosols, with Implications for Paleoweathering Conditions and Provenance. *Geol* 23, 921–924. doi:10.1130/0091-7613(1995)023<0921:uteopm>2.3.co;2

Feng, L., Li, C., Huang, J., Chang, H., and Chu, X. (2014). A Sulfate Control on marine Mid-depth Euxinia on the Early Cambrian (Ca. 529-521Ma) Yangtze Platform, South China. *Precambr. Res.* 246, 123–133. doi:10.1016/j.precamres.2014.03.002

Goldberg, T., Strauss, H., Guo, Q., and Liu, C. (2007). Reconstructing marine Redox Conditions for the Early Cambrian Yangtze Platform: Evidence from Biogenic sulphur and Organic Carbon Isotopes. *Palaeogeogr. Palaeoclimatol. Palaeoecol.* 254, 175–193. doi:10.1016/j.palaeo.2007.03.015

Guo, Q., Shields, G. A., Liu, C., Strauss, H., Zhu, M., Pi, D., et al. (2007). Trace Element Chemostratigraphy of Two Ediacaran-Cambrian Successions in South China: Implications for Organosedimentary Metal Enrichment and Silicification in the Early Cambrian. *Palaeogeogr. Palaeoclimatol. Palaeoecol.* 254, 194–216. doi:10.1016/j.palaeo.2007.03.016

Guo, Q., Strauss, H., Zhu, M., Zhang, J., Yang, X., Lu, M., et al. (2013). High Resolution Organic Carbon Isotope Stratigraphy from a Slope to Basinal Setting

on the Yangtze Platform, South China: Implications for the Ediacaran-Cambrian Transition. *Precambr. Res.* 225, 209–217. doi:10.1016/j.precamres.2011.10.003

He, T., Lu, S., Li, W., Sun, D., Pan, W., Zhang, B., et al. (2020a). Paleoweathering, Hydrothermal Activity and Organic Matter Enrichment during the Formation of Earliest Cambrian Black Strata in the Northwest Tarim Basin, China. *J. Pet. Sci. Eng.* 189, 106987. doi:10.1016/j.petrol.2020.106987

He, T. H., Lu, S. F., Li, W. H., Wang, W. M., Sun, D. Q., Pan, W. Q., et al. (2020b). Geochemical Characteristics and Effectiveness of Thick, Black Shales in Southwestern Depression, Tarim Basin. *J. Pet. Sci. Eng.* 185, 106607. doi:10.1016/j.petrol.2019.106607

Hou, M. C., Xing, F., Xu, S. L., Lin, L. B., Liu, X. C., Xiong, F. H., et al. (2017). Paleogeographic Patterns of E-C Transition Period in the Upper Yangtze and the Geodynamic Mechanism. *J. Acta Sedimentol. Sin.* 35 (5), 902–917. doi:10.14027/j.cnki.cjxb.2017.05.004

Hu, L., Zhu, Y. M., Chen, S. B., Chen, J., and Wang, Y. (2012). Resource Potential Analysis of Shale Gas in Lower Cambrian Qiongzhusi Formation in Middle & Upper Yangtze Region. J. *J. China Coal Soc.* 37 (11), 1871–1877. doi:10.13225/j.cnki.jccs.2012.11.003

Huang, J. L., Zou, C. N., Li, J. Z., Dong, D. Z., Wang, S. J., Wang, S. Q., et al. (2012). Shale Gas Generation and Potential of the Lower Cambrian Qiongzhusi Formation in Southern Sichuan Basin, China. J. *Pet. Explor. Develop.* 39 (01), 69–75. CNKI: SUN: SKYK. 0. 2012-01-009. doi:10.1016/s1876-3804(12)60017-2

Huang, J. Z. (1988). Classification Basis of Stable Carbon Isotope of Kerogen. J. *Geo. Ceochem.* 16 (3), 68–70.

Jiang, G., Sohl, L. E., and Christie-Blick, N. (2003). Neoproterozoic Stratigraphic Comparison of the Lesser Himalaya (India) and Yangtze Block (south China): Paleogeographic Implications. *Geol* 31 (10), 917–920. doi:10.1130/g19790.1

Jin, C., Li, C., Algeo, T. J., Wu, S., Cheng, M., Zhang, Z., et al. (2020). Controls on Organic Matter Accumulation on the Early-Cambrian Western Yangtze Platform, South China. *Mar. Pet. Geol.* 111, 75–87. doi:10.1016/j.marpetgeo.2019.08.005

Jones, C., and Manning, D. A. C. (1994). Comparison of Geochemical Indices Used for the Interpretation of Palaeoredox Conditions in Ancient Mudstones. *J. Chem. Geol.* 111, 111–136. doi:10.1016/0009-2541(94)90085-X

Kraal, P., Slomp, C. P., Forster, A., and Kuypers, M. M. M. (2010). Phosphorus Cycling from the Margin to Abyssal Depths in the Proto-Atlantic during Oceanic Anoxic Event 2. *Palaeogeogr. Palaeoclimatol. Palaeoecol.* 295, 42–54. doi:10.1016/j.palaeo.2010.05.014

Li, C., Shi, W., Cheng, M., Jin, C., and Algeo, T. J. (2020). The Redox Structure of Ediacaran and Early Cambrian Oceans and its Controls. *Sci. Bull.* 65, 2141–2149. doi:10.1016/j.scib.2020.09.023

Li, C. S. (1994). Origin of Lang Plants Is an Important Event of Life Evolution. *J. Bull. Natl. Nat. Sci. Found. China* 1994 (4), 7. doi:10.16262/j.cnki.1000-8217.1994.04.003

Li, W. H., Lu, S. F., Tan, Z. Z., and He, T. H. (2017). Lacustrine Source Rock Deposition in Response to Coevolution of the Paleoenvironment and Formation Mechanism of Organic-Rich Shales in the Biyang Depression. *Nanxiang Basin. J. Energ. Fuel.* 31, 13519–13527. doi:10.1021/acs.energyfuels.7b02880

Li, Z. X., Evans, D. A. D., and Halverson, G. P. (2013). Neoproterozoic Glaciations in a Revised Global Palaeogeography from the Breakup of Rodinia to the Assembly of Gondwanaland. *Sediment. Geology.* 294, 219–232. doi:10.1016/j.sedgeo.2013.05.016

Li, Z. W., Ran, B., Xiao, B., Song, J. M., Zheng, L., Li, J. X., et al. (2019). Sinian to Early Cambrian Uplift-Depression Framework along the Northern Margin of the Sichuan Basin, Central China and its Implications for Hydrocarbon Exploration. *J. Earth Sci. Front.* 26 (1), 59–85. doi:10.13745/j.esf.sf.2019.1.4

Li, Z. X., Bogdanova, S. V., Collins, A. S., Davidson, A., Waele, B. D., Ernst, R. E., et al. (2008). Assembly, Configuration, and Break-Up History of Rodinia: A Synthesis. *J. Precambrian Res.* 160 (1-2), 179–210. doi:10.1016/j.precamres.2007.04.021

Liang, X., Li, X. H., Xu, J. L., He, J., Han, Y. P., Cui, J., et al. (2021). Exploration Prospects of Lower Cambrian Shale Gas in the Central-Western Sichuan Basin under the Pattern of Tectonic-Depositional Differentiation: From High-Quality Source Rocks to Reservoirs. *J. Nat. Gas Industry.* 41 (5), 30–41. doi:10.3787/j.issn.1000-0979.2021.05.004

Liu, S. G., Sun, W., Luo, Z. L., Song, J., Zhong, Y., Tian, Y. H., et al. (2013). Xingkai Taphrogenesis and Petroleum Exploration from Upper Sinian to Cambrian Strata in Sichuan Basin, China. *J. Chengdu Univ. Technol. (Sci. Technol. ed.)* 40 (05), 511–520. doi:10.1016/s1876-3804(13)60043-9

Logan, G. A., Hayes, J. M., Hieshima, G. B., and Summons, R. E. (1995). Terminal Proterozoic Reorganization of Biogeochemical Cycles. *Nature* 376 (6535), 53–56. doi:10.1038/376053a0

Lu, S., Huang, W., Chen, F., Li, J., Wang, M., Xue, H., et al. (2012). Classification and Evaluation Criteria of Shale Oil and Gas Resources: Discussion and Application. *Pet. Exploration Dev.* 39, 268–276. doi:10.1016/S1876-3804(12)60042-1

März, C., Poulton, S. W., Beckmann, B., Küster, K., Wagner, T., and Kasten, S. (2008). Redox Sensitivity of P Cycling during Marine Black Shale Formation: Dynamics of Sulfidic and Anoxic, Non-sulfidic Bottom Waters. *Geochim. Cosmochim. Acta* 72, 3703–3717. doi:10.1016/j.gca.2008.04.025

Murray, R. W., and Leinen, M. (1996). Scavenged Excess Aluminum and its Relationship to Bulk Titanium in Biogenic Sediment from the central Equatorial Pacific Ocean. *Geochim. Cosmochim. Acta* 60, 3869–3878. doi:10.1016/0016-7037(96)00236-0

Nesbitt, H. W., and Young, G. M. (1982). Early Proterozoic Climates and Plate Motions Inferred from Major Element Chemistry of Lutites. *Nature* 299, 715–717. doi:10.1038/299715a0

Nesbitt, H. W., Young, G. M., Mclennan, S. M., and Keays, R. R. (1996). Effects of Chemical Weathering and Sorting on the Petrogenesis of Siliciclastic Sediments, with Implications for Provenance Studies. *J. Geology.* 104 (5), 525–542. doi:10.1086/629850

Och, L. M., Shields-Zhou, G. A., Poulton, S. W., Manning, C., Thirlwall, M. F., Li, D., et al. (2013). Redox Changes in Early Cambrian Black Shales at Xiaotan Section, Yunnan Province, South China. *Precambr. Res.* 225, 166–189. doi:10.1016/j.precamres.2011.10.005

Parker, A. (1970). An Index of Weathering for Silicate Rocks. *Geol. Mag.* 107, 501–504. doi:10.1017/S0016756800058581

Peters, K. E., and Cassa, M. R. (1994). Applied Source Rock Geochemistry. *AAPG Mem.* 60, 93–120.

Peters, K. E., Walters, C. C., and Moldowan, J. M. (2005). *The Biomarker Guide: Biomarkers and Isotopes in Petroleum Exploration and Earth History*. Cambridge: Cambridge University Press.

Pi, D. H., Liu, C. Q., Shields-Zhou, G. A., and Jiang, S. Y. (2013). Trace and Rare Earth Element Geochemistry of Black Shale and Kerogen in the Early Cambrian Niutitang Formation in Guizhou Province, South China: Constraints for Redox Environments and Origin of Metal Enrichments. *Precambrian Res.* 225, 218–229. doi:10.1016/j.precamres.2011.07.004

Piper, D. Z., and Dean, W. E. (2002). Trace-Element Deposition in the Cariaco Basin, Venezuela Shelf, under Sulfate-Reducing Conditions: A History of the Local Hydrography and Global Climate, 20 Ka to the Present. *US Geol. Surv.* doi:10.3133/pp1670

Raven, M. R., Keil, R. G., and Webb, S. M. (2021). Microbial Sulfate Reduction and Organic Sulfur Formation in Sinking Marine Particles. *Science* 371 (6525), 178–181. doi:10.10.1126/science.abc6035

Reinhard, C. T., Planavsky, N. J., Gill, B. C., Ozaki, K., Robbins, L. J., Lyons, T. W., et al. (2016). Evolution of the Global Phosphorus Cycle. *Nature* 541, 386–389. doi:10.1038/nature2077210.1038/nature20772

Schoepfer, S. D., Shen, J., Wei, H., Tyson, R. V., Ingall, E., and Algeo, T. J. (2015). Total Organic Carbon, Organic Phosphorus, and Biogenic Barium Fluxes as Proxies for Paleomarine Productivity. *Earth-Science Rev.* 149, 23–52. doi:10.1016/j.earscirev.2014.08.017

Scott, C., Lyons, T. W., Bekker, A., Shen, Y., Poulton, S. W., Chu, X., et al. (2008). Tracing the Stepwise Oxygenation of the Proterozoic Ocean. *Nature* 452, 456–459. doi:10.1038/nature06811

Shen, J., Schoepfer, S. D., Feng, Q., Zhou, L., Yu, J., Song, H., et al. (2015). Marine Productivity Changes during the End-Permian Crisis and Early Triassic Recovery. *Earth-Science Rev.* 149, 136–162. doi:10.1016/j.earscirev.2014.11.002

Shu, D., Isozaki, Y., Zhang, X., Han, J., and Maruyama, S. (2014). Birth and Early Evolution of Metazoans. *Gondwana Res.* 25 (3), 884–895. doi:10.1016/j.gr.2013.09.001

Spangenberg, J. E., Bagnoud-Velásquez, M., Boggiani, P. C., and Gaucher, C. (2014). Redox Variations and Bioproductivity in the Ediacaran: Evidence from Inorganic and Organic Geochemistry of the Corumbá Group, Brazil. *Gondwana Res.* 26, 1186–1207. doi:10.1016/j.gr.2013.08.014

Srivastava, P., Siva Siddaiah, N., Sangode, S. J., and Meshram, D. C. (2018). Mineralogy and Geochemistry of Various Colored Boles from the Deccan Volcanic Province: Implications for Paleoweathering and Paleoenvironmental Conditions. *Catena* 167, 44–59. doi:10.1016/j.catena.2018.04.024

Stroobants, N., Dehairs, F., Goeyens, L., Vanderheijden, N., and Van Grieken, R. (1991). Barite Formation in the Southern Ocean Water Column. *Mar. Chem.* 35, 411–421. doi:10.1016/s0304-4203(09)90033-0

Sun, W., Liu, S., Ran, B., Wang, S., Ye, Y., Luo, C., et al. (2012). General Situation and Prospect Evaluation of the Shale Gas in Niutitang Formation of Sichuan Basin and its Surrounding Areas. J. *J. Chengdu Univ. Technol. (Science Technol. edition)* 39 (02), 170–175. doi:10.3969/j.issn.1671-9727.2012.02.009

Sweere, T., van den Boorn, S., Dickson, A. J., and Reichart, G.-J. (2016). Definition of New Trace-Metal Proxies for the Controls on Organic Matter Enrichment in Marine Sediments Based on Mn, Co, Mo and Cd Concentrations. *Chem. Geology.* 441, 235–245. doi:10.1016/j.chemgeo.2016.08.028

Taylor, S. R., and Mclennan, S. M. (1985). *The Continental Crust: Its Composition and Evolution*. Oxford, U.K: Blackwell Scientific Publications, 1–312.

TengerLiu, W. H., Xu, Y. C., and Chen, J. F. (2004). Organic Carbon Isotope Record in marine Sediment and its Environmental Significance-An Example from Ordos Basin,NW China. J. *Petrol. Explor. Dev.* 31 (5), 11–16. doi:10.3321/j.issn:1000-0747.2004.05.003

Von Breymann, M. T., Emeis, K.-C., and Suess, E. (1992). Water Depth and Diagenetic Constraints on the Use of Barium as a Palaeoproductivity Indicator. *Geol. Soc. Lond. Spec. Publ.* 64, 273–284. doi:10.1144/gsl.sp.1992.064.01.18

Wang, H. (2020). *Sedimentary Structural Pattern and its Significance of Petroleum Geology from Sinian to Early Cambrian in Northern Margin of Upper Yangtze [D]*. Chengdu: Chengdu University of Technology, 2–5. (In Chinese with English abstract).

Wang, R., Xu, Z., Santosh, M., Yao, Y., Gao, L. e., and Liu, C. (2016). Late Neoproterozoic Magmatism in South Qinling, Central China: Geochemistry, Zircon U-Pb-Lu-Hf Isotopes and Tectonic Implications. *Tectonophysics* 683, 43–61. doi:10.1016/j.tecto.2016.05.050

Wang, S., Zou, C., Dong, D., Wang, Y., Li, X., Huang, J., et al. (2015). Multiple Controls on the Paleoenvironment of the Early Cambrian Marine Black Shales in the Sichuan Basin, SW China: Geochemical and Organic Carbon Isotopic Evidence. *Mar. Pet. Geology.* 66, 660–672. doi:10.1016/j.marpetgeo.2015.07.009

Westermann, S., Stein, M., Matera, V., Fiet, N., Fleitmann, D., Adatte, T., et al. (2013). Rapid Changes in the Redox Conditions of the Western Tethys Ocean during the Early Aptian Oceanic Anoxic Event. *Geochim. et Cosmochim. Acta* 121, 467–486. doi:10.1016/j.gca.2013.07.023

Xiao, S., Zhang, Y., and Knoll, A. H. (1998). Three-Dimensional Preservation of Algae and Animal Embryos in A Neoproterozoic Phosphorite. *Nature* 391, 553–558. doi:10.1038/35318

Yao, W. H., Li, Z. X., Li, W. X., Su, L., and Yang, J. H. (2015). Detrital Provenance Evolution of the Ediacaran-Silurian Nanhua Foreland basin, South China. *Gondwana Res.* 28 (4), 1449–1465. doi:10.1016/j.gr.2014.10.018

Zhai, L., Wu, C., Ye, Y., Zhang, S., and An, Z. (2016). Marine Redox Variations during the Ediacaran-Cambrian Transition on the Yangtze Platform, South China. *Geol. J.* 53, 58–79. doi:10.1002/gj.2878

Zhang, B., Yao, S., Wignall, P. B., Hu, W., Ding, H., Liu, B., et al. (2018). Widespread Coastal Upwelling along the Eastern Paleo-Tethys Margin (South China) during the Middle Permian (Guadalupian): Implications for Organic Matter Accumulation. *Mar. Pet. Geology.* 97, 113–126. doi:10.1016/j.marpetgeo.2018.06.025

Zhang, J., Fan, T., Algeo, T. J., Li, Y., and Zhang, J. (2016). Paleo-marine Environments of the Early Cambrian Yangtze Platform. *Palaeogeogr. Palaeoclimatol. Palaeoecol.* 443, 66–79. doi:10.1016/j.palaeo.2015.11.029

Zhang, K., Jia, C., Song, Y., Jiang, S., Jiang, Z., Wen, M., et al. (2020). Analysis of Lower Cambrian Shale Gas Composition, Source and Accumulation Pattern in Different Tectonic Backgrounds: A Case Study of Weiyuan Block in the Upper Yangtze Region and Xiuwu Basin in the Lower Yangtze Region. *Fuel* 263, 115978. doi:10.1016/j.fuel.2019.115978

Zhang, S. C., Liang, D. G., and Zhang, D. J. (2002). Evaluation Criteria for Paleozoic Effective Hydrocarbon Source Rocks. J. *Petrol. Explor. Dev.* 29 (2), 8–12. doi:10.3321/j.issn:1000-0747.2002.02.002

Zhang, Z. L., Wu, L. Y., Tuo, Q., and Shu, N. Z. (2007). Abnormal Value Recovery of Maturity Parameter Tmax for Rock-Eval. J. *Petrol. Explor. Dev.* 34 (5), 580–584.

Zhao, K., Li, T., Zhu, G., Zhang, Z., Li, J., Wang, P., et al. (2020). Geochemical Characteristics and Formation Mechanism of High-Quality Lower Cambrian Source Rocks: A Case Study of the Tianzhushan Profile in Western Hubei. *J. Acta Petrolei Sinica.* 41 (01), 13–26.

Zhou, G. X., Wei, G. Q., Hu, G. Y., Wu, S. J., Tian, Y. J., and Dong, C. Y. (2020). The Development Setting and the Organic Matter Enrichment of the Lower Cambrian Shales from the Western Rift Trough in Sichuan Basin. J. *Nat. Gas Geosci.* 31 (4), 498–506. doi:10.11764/j.issn.1672-1926.2019.11.013

Zhu, B., Jiang, S., Pi, D., Ge, L., and Yang, J. (2018). Trace Elements Characteristics of Black Shales from the Ediacaran Doushantuo Formation, Hubei Province, South China: Implications for Redox and Open vs. Restricted Basin Conditions. J. *J. Earth Sci.* 29 (02), 342–352. CNKI: SUN: ZDDY.0. 2018-02-009. doi:10.1007/s12583-017-0907-5

Zhu, M., Gehling, J. G., Xiao, S., Zhao, Y., and Droser, M. L. (2008). Eight-Armed Ediacara Fossil Preserved in Contrasting Taphonomic Windows from China and Australia. *Geol* 36 (11), 867–870. doi:10.1130/G25203A.110.1130/g25203a.1

Conflict of Interest: The authors declare that the research was conducted in the absence of any commercial or financial relationships that could be construed as a potential conflict of interest.

Publisher's Note: All claims expressed in this article are solely those of the authors and do not necessarily represent those of their affiliated organizations, or those of the publisher, the editors and the reviewers. Any product that may be evaluated in this article, or claim that may be made by its manufacturer, is not guaranteed or endorsed by the publisher.